UPF3A and UPF3B are redundant and modular activators of nonsense-mediated mRNA decay in human cells

Damaris Wallmeroth[1,2], Volker Boehm[1,2], Jan-Wilm Lackmann[3], Janine Altmüller[4,5], Christoph Dieterich[6,7], Niels H. Gehring[1,2]

1 Institute for Genetics, University of Cologne, 50674 Cologne, Germany

2 Center for Molecular Medicine Cologne (CMMC), University of Cologne, 50937 Cologne, Germany

3 CECAD Research Center, University of Cologne, Joseph-Stelzmann-Str. 26, 50931 Cologne, Germany

4 Cologne Center for Genomics (CCG), University of Cologne, 50931 Cologne, Germany

5 Present address: Berlin Institute of Health at Charité – Universitätsmedizin Berlin, Core Facility Genomics, Charitéplatz 1, 10117 Berlin, Germany and Max Delbrück Center for Molecular Medicine in the Helmholtz Association (MDC), Berlin, Germany

6 Section of Bioinformatics and Systems Cardiology, Department of Internal Medicine III and Klaus Tschira Institute for Integrative Computational Cardiology, Heidelberg University Hospital, 69120 Heidelberg, Germany

7 DZHK (German Centre for Cardiovascular Research), Partner site Heidelberg/Mannheim, 69120 Heidelberg, Germany

*Correspondence: boehmv@uni-koeln.de (V.B.), ngehring@uni-koeln.de (N.H.G.)

Keywords

Nonsense-mediated mRNA decay, gene paralogs, mRNA turnover, UPF3

Abstract

The paralogous human proteins UPF3A and UPF3B are involved in recognizing mRNAs targeted by nonsense-mediated mRNA decay (NMD). While UPF3B has been demonstrated to support NMD, contradicting reports describe UPF3A either as an NMD activator or inhibitor. Here, we present a comprehensive functional analysis of UPF3A and UPF3B in human cells using combinatory experimental approaches. Overexpression or knockout of UPF3A as well as knockout of UPF3B did not detectably change global NMD activity. In contrast, the co-depletion of UPF3A and UPF3B resulted in a marked NMD inhibition and a transcriptome-wide upregulation of NMD substrates, demonstrating a functional redundancy between both NMD factors. Although current models assume that UPF3 bridges NMD-activating exon-junction complexes (EJC) to the NMD factor UPF2, UPF3B exhibited only slightly impaired NMD activity in rescue experiments when UPF2 or EJC binding was impaired. Further rescue experiments revealed partially redundant functions of UPF3B domains in supporting NMD, involving both UPF2 and EJC interaction sites and the central region of UPF3. Collectively, UPF3A and UPF3B serve as fault-tolerant NMD activators in human cells.

43 ## Introduction

44 Precisely regulated expression of correct gene products is indispensable for eukaryotic life.
45 This is underlined by the existence of several quality control mechanisms for gene expression,
46 one of which is the nonsense-mediated mRNA decay (NMD). NMD is primarily known for its
47 ability to eliminate mature mRNAs that contain a premature termination codon (PTC). Thereby,
48 NMD prevents the synthesis and accumulation of C-terminally truncated proteins, which may
49 possess undesirable and potentially disease-causing properties (Frischmeyer & Dietz, 1999).
50 Although the removal of PTC-containing mRNAs was initially considered the most important
51 function of NMD, later studies showed that NMD plays an important role in the post-
52 transcriptional regulation of a substantial part of the transcriptome (He *et al.*, 2003; Lelivelt &
53 Culbertson, 1999; Mendell *et al.*, 2004; Rehwinkel *et al.*, 2005). The importance of the factors
54 involved in NMD is underscored by the severe impact that mutations in components of this
55 machinery have on development in metazoans, up to causing embryonic lethality in mammals
56 (Hwang & Maquat, 2011; Li *et al.*, 2015; McIlwain *et al.*, 2010; Medghalchi *et al.*, 2001;
57 Metzstein & Krasnow, 2006; Weischenfeldt *et al.*, 2008; Wittkopp *et al.*, 2009).

58 The final step of gene expression is the cytoplasmic translation of the mRNA by ribosomes.
59 Previous studies suggested that prolonged ribosome stalling at a termination codon indicates
60 improper translation termination and thereby triggers NMD (Amrani *et al.*, 2004; Peixeiro *et al.*,
61 2012). This could be caused by a long 3' untranslated region (UTR) that increases the distance
62 between the stalled ribosome and the poly(A)-binding protein (PABPC1), which normally
63 promotes proper translation termination (Amrani *et al.*, 2004). Alternatively, NMD can also be
64 activated by any PTC located more than 50-55 nt upstream of the 3'-most exon-exon junction.
65 Transcripts with such a PTC may be transcribed from mutant genes with nonsense mutations
66 but could also be generated by defective or alternative splicing (Kervestin & Jacobson, 2012).
67 The aforementioned 50-55 nt boundary between NMD-activating and NMD-resistant PTCs is
68 determined by the RNA-binding exon junction complex (EJC), which is deposited by the
69 spliceosome 20-24 nt upstream of every spliced exon-exon junction (Le Hir *et al.*, 2000). The

70 EJCs remain attached on the mature mRNA during export into the cytoplasm, where they are
71 removed by translating ribosomes or the disassembly factor PYM1 (Dostie & Dreyfuss, 2002;
72 Le Hir *et al.*, 2000). If translation terminates prematurely due to the presence of a PTC, EJCs
73 bound downstream of the PTC serve as a marker for the NMD machinery and the initial
74 activation of NMD (Kim *et al.*, 2001; Le Hir *et al.*, 2001).

75 Extensive research over many decades has resulted in a model for EJC-dependent NMD.
76 According to this model, the central factor UPF1 is bound non-specifically to all present
77 transcripts in the cell and is removed from the coding sequence by translating ribosomes (Hogg
78 & Goff, 2010; Hurt *et al.*, 2013; Kurosaki & Maquat, 2013; Zund *et al.*, 2013). If translation
79 terminates prematurely, UPF1 interacts with the stalled ribosome and serves as the anchoring
80 point for the other NMD factors. The presence of a downstream EJC is detected by the
81 interaction of UPF1 with UPF2, which in turn binds to UPF3. The latter can bind directly to the
82 EJC, resulting in a bridged connection of UPF1 to the EJC (Chamieh *et al.*, 2008; Kim *et al.*,
83 2001; Le Hir *et al.*, 2001; Weng *et al.*, 1996). This series of interactions marks the termination
84 codon as premature and stimulates the phosphorylation of N- and C-terminal SQ motif-
85 containing regions of UPF1 by the kinase SMG1 (Yamashita *et al.*, 2001). In its phosphorylated
86 state UPF1 recruits the heterodimer SMG5-SMG7 and/or SMG6, which are responsible for
87 both exoribonucleolytic and endoribonucleolytic degradation of the mRNA, respectively
88 (Boehm *et al.*, 2021; Chen & Shyu, 2003; Lejeune *et al.*, 2003). The endonuclease SMG6
89 cleaves the mRNA in close proximity to the PTC, resulting in two mRNA fragments (Eberle *et*
90 *al.*, 2009) of which the 3' fragment is degraded by the 5'-to-3' exoribonuclease XRN1 (Eberle
91 *et al.*, 2009; Huntzinger *et al.*, 2008).

92 The protein UPF3 plays an important role in the NMD pathway. As detailed above, its main
93 function is believed to bridge the NMD machinery to the EJC providing a physical link between
94 UPF2 and the EJC (Chamieh *et al.*, 2008; Kashima *et al.*, 2006; Lykke-Andersen *et al.*, 2000;
95 Serin *et al.*, 2001). With its conserved RNA recognition motif (RRM) in the N-terminus, UPF3
96 can interact with the C-terminal MIF4G (middle portion of eIF4G) domain of UPF2 (Kadlec *et*

97 *al.*, 2004). The association with the EJC-binding site, formed by the core components EIF4A3,
98 MAGOHB and RBM8A, is enabled by a C-terminal sequence referred to as EJC binding motif
99 (EBM) (Buchwald *et al.*, 2010; Gehring *et al.*, 2003; Kim *et al.*, 2001).

100 In vertebrates two genes encode for two UPF3 paralogues: UPF3A and UPF3B, each of which
101 expressing two different isoforms generated by alternative splicing (Lykke-Andersen *et al.*,
102 2000; Serin *et al.*, 2001). Both human UPF3 proteins contain the same important domains, but
103 differ in details regarding their interactions. According to previous studies, UPF3A and UPF3B
104 are in constant competition for their binding partner UPF2. However, UPF3B binds tighter to
105 UPF2 than UPF3A and therefore UPF3A gets destabilized, and its protein levels are barely
106 detectable under normal conditions (Chan *et al.*, 2009).

107 Recently, UPF3B was reported to interact with the eukaryotic release factor 3 (eRF3) via the
108 so far uncharacterized middle domain (amino acids (aa) 147-256) (Neu-Yilik *et al.*, 2017). Due
109 to this interaction and binding of the terminating ribosome, it can delay translation termination,
110 which is known to define aberrant termination events and trigger NMD (Amrani *et al.*, 2004;
111 Neu-Yilik *et al.*, 2017; Peixeiro *et al.*, 2012).

112 Due to the different molecular characteristics of the UPF3 paralogs, their exact role in NMD is
113 a long-discussed topic. On the one hand, previous studies showed that UPF3A and UPF3B
114 both trigger degradation of a reporter construct when tethered downstream of a termination
115 codon. Notably, the efficiency of UPF3A to elicit NMD was weaker in comparison to UPF3B,
116 which was attributed to a weaker interaction with the EJC (Kunz *et al.*, 2006; Lykke-Andersen
117 *et al.*, 2000). This would suggest that, at least with respect to their NMD activity, UPF3A and
118 UPF3B serve a similar, perhaps even redundant, function. This notion is supported by the
119 observation that in patients with mutated UPF3B the amount of stabilized UPF3A inversely
120 correlated with the severity of the patients' clinical phenotypes (Nguyen *et al.*, 2012). On the
121 other hand, it was recently reported that loss of UPF3A results in increased transcript
122 destabilization, and UFP3A overexpression in NMD inhibition (Shum *et al.*, 2016). This would

123 rather indicate opposing functions of the two UPF3 paralogs with UPF3A being an antagonist
124 of UPF3B and broadly acting as an NMD inhibitor.

125 In this study, we resolved the controversy about the functions of UPF3A and UPF3B in the
126 NMD pathway using different UPF3 overexpression and knockout (KO) HEK293 cell lines. We
127 found that neither overexpression nor genomic KO of UPF3A resulted in substantial changes
128 of NMD activity or global alterations of the transcriptome. In UPF3B KO cells UPF3A protein
129 levels were upregulated, but NMD activity was maintained at almost normal level. In contrast,
130 the co-depletion of both UPF3 paralogs resulted in a marked NMD inhibition and a global
131 upregulation of PTC-containing transcripts. Moreover, rescue experiments revealed that UPF3
132 proteins have additional functions besides bridging the EJC and the NMD machinery. Taken
133 together, our data support a model of human NMD, in which UPF3A and UPF3B can replace
134 each other and therefore perform redundant functions.

135 # RESULTS

136 ## UPF3A overexpression or knockout does not affect NMD efficiency

137 Prior work using different mammalian models and various experimental approaches reached
138 different conclusions regarding the function of UPF3A in NMD (Fig 1A). Therefore, we set out
139 to re-examine the role of UPF3A in human cells by specifically manipulating its expression
140 levels. Under regular conditions UPF3A is barely present in cultured cells, presumably due to
141 its lower binding affinity to the stabilizing interaction partner UPF2 compared to UPF3B,
142 resulting in a rapid turnover of "free" UPF3A (Chan *et al.*, 2009). We hypothesized that
143 increasing the abundance of UPF3A should lead to the stabilization of NMD targets if UPF3A
144 is an NMD inhibitor. To test this hypothesis, we generated Flp-In T-REx 293 (HEK293) cells
145 inducibly overexpressing FLAG-tagged wildtype UPF3A to high protein levels (Fig 1B). Global
146 analysis of the transcriptome using RNA-seq (Fig EV1A and Datasets EV1-EV3) revealed,
147 except for UPF3A itself, no significant differential gene expression (DGE), differential transcript
148 usage (DTU) or alternative splicing (AS) events upon UPF3A overexpression compared to
149 control conditions (Figs 1C and D). Using these RNA-seq data, we analyzed NMD targets that
150 were previously described to be strongly upregulated in UPF3A overexpressing HeLa cells
151 (Shum *et al.*, 2016). The DGE analysis and visualization of the respective read coverage
152 showed no substantial effects in our setup (Figs 1E and EV1B-E). Furthermore, quantification
153 of differential transcript usage via IsoformSwitchAnalyzeR (Vitting-Seerup & Sandelin, 2019)
154 could neither detect any differences in the global isoform fraction distribution, nor an
155 accumulation of PTC-containing transcripts (Fig EV1F). Collectively, these analyses indicated
156 that UPF3A overexpression in HEK293 cells does not negatively affect gene expression in
157 general or NMD in particular.

A

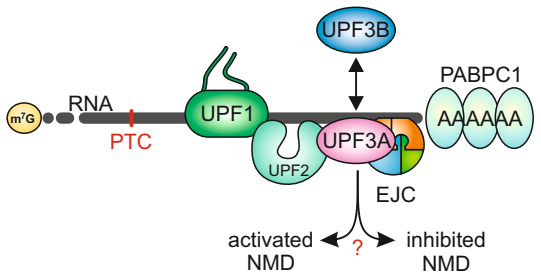

B

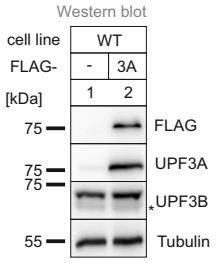

C

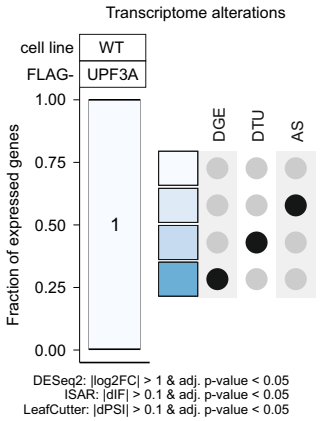

D

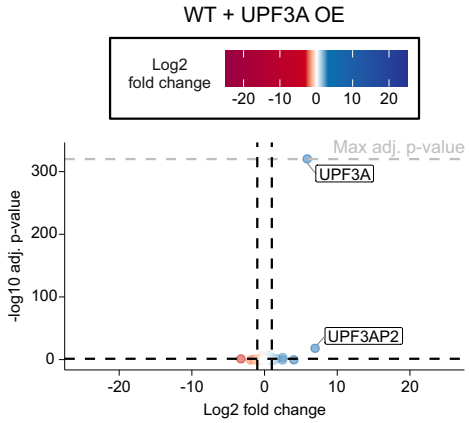

E

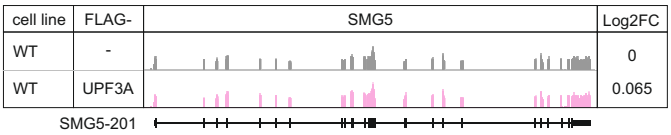

Figure 1 - UPF3A overexpression does not affect NMD
A Schematic representation of the bridge between UPF1 and the EJC during NMD. Binding of UPF3A instead of the stronger bound UPF3B is discussed to either activate or inhibit NMD.
B Western blot analyses after induced expression of FLAG-tagged UPF3A in WT HEK 293 cells. Tubulin serves as control. The asterisk indicates unspecific bands.
C Fraction of expressed genes (genes with non-zero counts in DESeq2) were calculated which exhibit individual or combinations of differential gene expression (DGE), differential transcript usage (DTU) and/or alternative splicing (AS) events in WT cells overexpressing UPF3A using the respective computational analysis (cutoffs are indicated). AS and DTU events were collapsed on the gene level. For DGE, p-values were calculated by DESeq2 using a two-sided Wald test and corrected for multiple testing using the Benjamini-Hochberg method. For DTU, p-values were calculated by IsoformSwitchAnalyzeR (ISAR) using a DEXSeq-based test and corrected for multiple testing using the Benjamini-Hochberg method. For AS, p-values were calculated by LeafCutter using an asymptotic Chi-squared distribution and corrected for multiple testing using the Benjamini-Hochberg method.
D Volcano plot showing the differential gene expression analyses from the RNA-Seq dataset of WT cells overexpressing UPF3A. The log2 fold change is plotted against the -log10 adjusted p-value (adj. p-value). P-values were calculated by DESeq2 using a two-sided Wald test and corrected for multiple testing using the Benjamini-Hochberg method. OE = overexpression.
E Read coverage of SMG5 from WT HEK 293 RNA-seq data with or without induced UPF3A overexpression shown as Integrative Genomics Viewer (IGV) snapshot. Differential gene expression (from DESeq2) is indicated as Log2 fold change (Log2FC) on the right. Schematic representation of the protein coding transcript below.

159 Next, we approached the question of UPF3A function in the opposite way by generating
160 UPF3A knockout (KO) HEK293 cell lines. Using CRISPR-Cas9 genome editing we isolated
161 three clones that lacked the UPF3A-specific band on the Western blot even after
162 downregulation of UPF3B (Fig 2A). Two clones (14 and 20) were characterized in detail.

163 In both cell lines, the UPF3A genomic locus contained insertions and/or deletions causing
164 frame-shifts and eventually PTCs (Figs EV2A-C). To gain a first impression of the NMD activity
165 in the UPF3A KO cells, the transcript levels of three known exemplary endogenous NMD
166 targets, RSRC2, SRSF2 and ZFAS1 were determined by qPCR (Boehm *et al.*, 2021; Lykke-
167 Andersen *et al.*, 2014; Sureau *et al.*, 2001). WT HEK293 cells treated with SMG6 and SMG7
168 siRNAs were used as a positive control for severe NMD inhibition (Fig 2B)(Boehm *et al.*, 2021).
169 While the absence of UPF3A did not result in abundance changes of SRSF2 and RSRC2
170 NMD-sensitive isoforms (mean log2FC between -0.44 and 0.79), ZFAS1 mRNA levels were
171 slightly decreased in the UPF3A KO cells compared to WT cells (mean log2FC -0.42 and -1.01
172 for UPF3A KO clones 14 and 20, respectively; Fig 2B). However, this effect was not rescued
173 by the (over)expression of transgenic UPF3A, indicating that it is not caused by the lack of
174 UPF3A but rather represents random variations in gene expression or clonal effects (Figs
175 EV2D-E). To get a complete overview of the effects of the UPF3A KO, we performed RNA-seq
176 of two UPF3A KO cell lines with or without an additional UPF3B knockdown (KD; Fig EV2F
177 and Datasets EV1-EV3). Initially, we focused on the UPF3A KO cell lines without KDs, for
178 which the global transcriptome analysis revealed that about 4-9 % of the expressed genes are
179 altered (Figs 2C-E). The observation that in the absence of UPF3A more genes were
180 downregulated than upregulated (1002 vs. 886) could be an indicator for UPF3A NMD
181 inhibiting properties (Fig 2F). However, the majority of genes with altered expression were
182 clone specific and only 120 genes showed downregulation in both UPF3A KO cell lines (Fig
183 2F). Investigation of selected targets that were significantly up- or downregulated in both clones
184 revealed that the changes were not rescued after UPF3A overexpression, suggesting that they
185 are UPF3A-independent (Figs EV2D-E). Another indication that UPF3A depletion does not
186 generally affect NMD efficiency came from the DTU analysis.

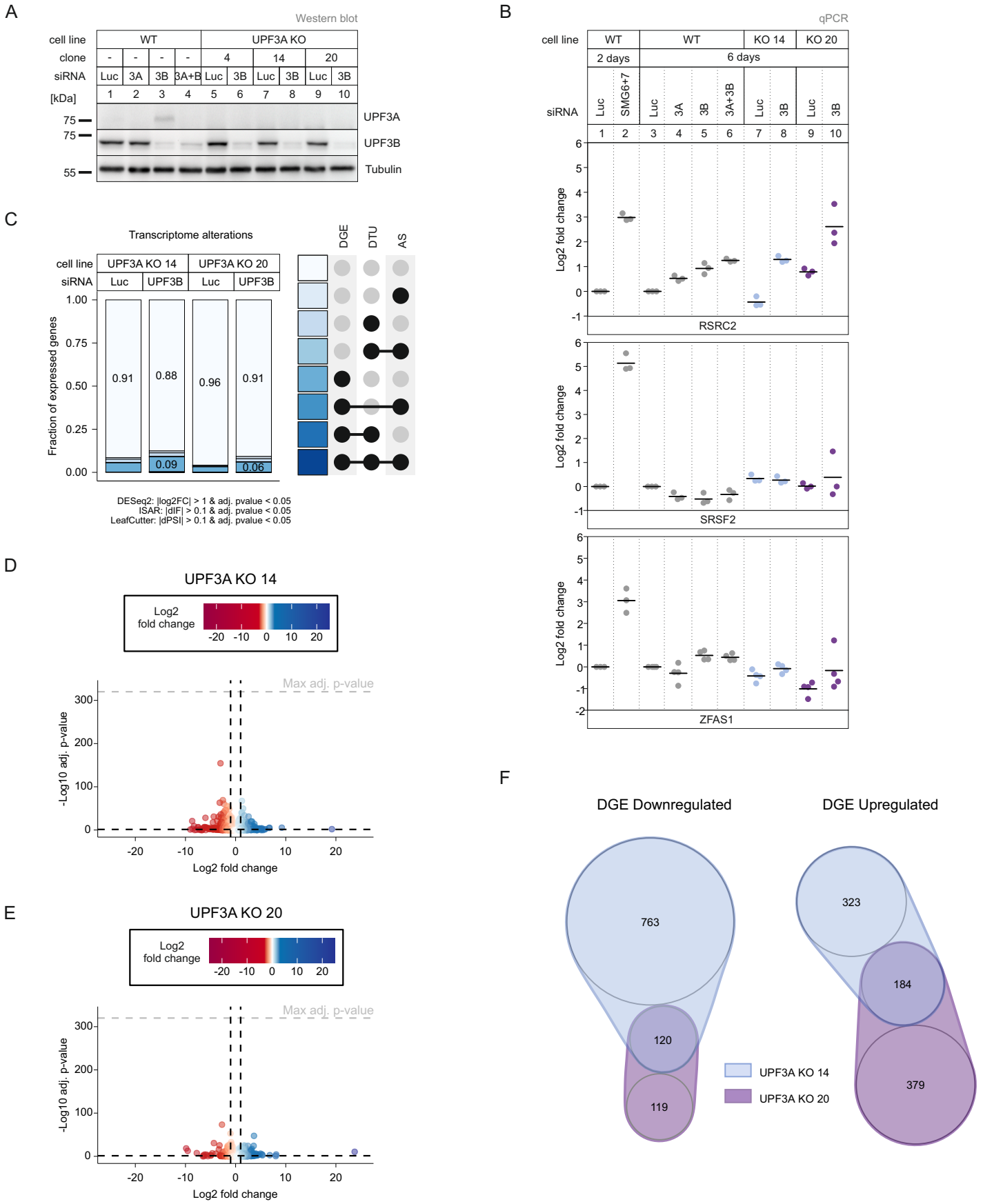

Figure 2 - UPF3A KOs show light NMD-independent transcriptome alterations

A Western blot analysis of WT and UPF3A KO cells (clones 4, 14 and 20) with the indicated siRNA treatments. UPF3A and UPF3B protein levels were detected, Tubulin serves as control.

B Quantitative RT-PCR of the indicated cell lines treated with the indicated siRNAs for 2 or 6 days. For RSRC2 and SRSF2 the ratio of NMD isoform to canonical isoform was calculated. ZFAS1 expression was normalized to C1orf43 reference. Data points and means are plotted as Log2 fold change (n=3 for RSRC2 and SRSF2, n=4 for ZFAS1).

C Fraction of expressed genes (genes with non-zero counts in DESeq2) were calculated which exhibit individual or combinations of differential gene expression (DGE), differential transcript usage (DTU) and/or alternative splicing (AS) events in the indicated conditions using the respective computational analysis (cutoffs are indicated). AS and DTU events were collapsed on the gene level. For DGE, p-values were calculated by DESeq2 using a two-sided Wald test and corrected for multiple testing using the Benjamini-Hochberg method. For DTU, p-values were calculated by IsoformSwitchAnalyzeR using a DEXSeq-based test and corrected for multiple testing using the Benjamini-Hochberg method. For AS, p-values were calculated by LeafCutter using an asymptotic Chi-squared distribution and corrected for multiple testing using the Benjamini-Hochberg method.

D,E Volcano plots showing the differential gene expression analyses from the indicated RNA-Seq datasets (D UPF3A KO clone 14, E UPF3A KO clone 20). The log2 fold change is plotted against the -log10 adjusted p-value (padj). P-values were calculated by DESeq2 using a two-sided Wald test and corrected for multiple testing using the Benjamini-Hochberg method

F nVenn Diagram showing the overlap of up- or downregulated genes in the UPF3A KO cell lines 14 and 20. Log2 fold change <1 (downregulated) or >1 (upregulated) and adjusted p-value (padj) < 0.05. DGE = Differential Gene Expression.

188 Although clone 14 showed a minor downregulation of PTC-containing transcripts, which could
189 indicate more active NMD, this effect was not reproducible in the second clone (Fig EV2G). In
190 view of and in combination with the results shown in Fig 1, this strongly suggests that neither
191 the overexpression nor the depletion of UPF3A substantially alters (negatively or positively)
192 the efficiency of NMD. In conclusion, our data argue against a role for UPF3A as a general
193 negative NMD regulator in human cell lines.

194 **NMD is functional in the absence of UPF3B**

195 Next, we investigated the RNA-seq data of UPF3B knockdowns in the UPF3A KO cells
196 (Datasets EV1-EV3). We observed that this combination resulted in more transcriptome
197 alterations and an increase of PTC-containing isoforms (Figs 2B-C, EV2H and I). Although the
198 UPF3B KD alone could be in principle responsible for this effect, the results could also be an
199 indicator for redundant functions of the two UPF3 paralogs. To explore this hypothesis, we
200 decided to generate UPF3B KO cell lines. Western blot analysis demonstrated that a UPF3B
201 KD is less efficient in reducing the produced protein than the UPF3B KO in the two clones
202 designated as 90 and 91 (Figs 3A and EV3A-B). In addition, we observed a strong upregulation
203 of UPF3A after depletion (KO) or reduction (KD) of UPF3B, as described before (Chan *et al.*,
204 2009). In the absence of UPF3B no changes in the expression of the respective NMD-sensitive
205 isoforms of the NMD-targets RSRC2 and SRSF2 was observed (Fig 3B). This indicates that
206 either UPF3B is not essential for NMD or that another protein is able to compensate for its
207 loss. The most obvious candidate for this function is its own paralog UPF3A, which was also
208 suggested previously to functionally replace UPF3B in NMD. Indeed, knocking down UPF3A
209 in the UPF3B KO cells resulted in the increase of NMD-sensitive RSRC2 and SRSF2 isoforms
210 (Fig 3B). Of note, the combination of the UPF3B KO with UPF3A KD showed stronger effects
211 than the previously analyzed UPF3A KO plus UPF3B KD. This is probably caused by the lower
212 KD efficiency of the UPF3B siRNAs which can be observed by comparing the respective
213 protein levels (Fig 2A vs. Fig 3A). We suspect that the remaining UPF3B levels after siRNA-
214 mediated UPF3B KD still support NMD.

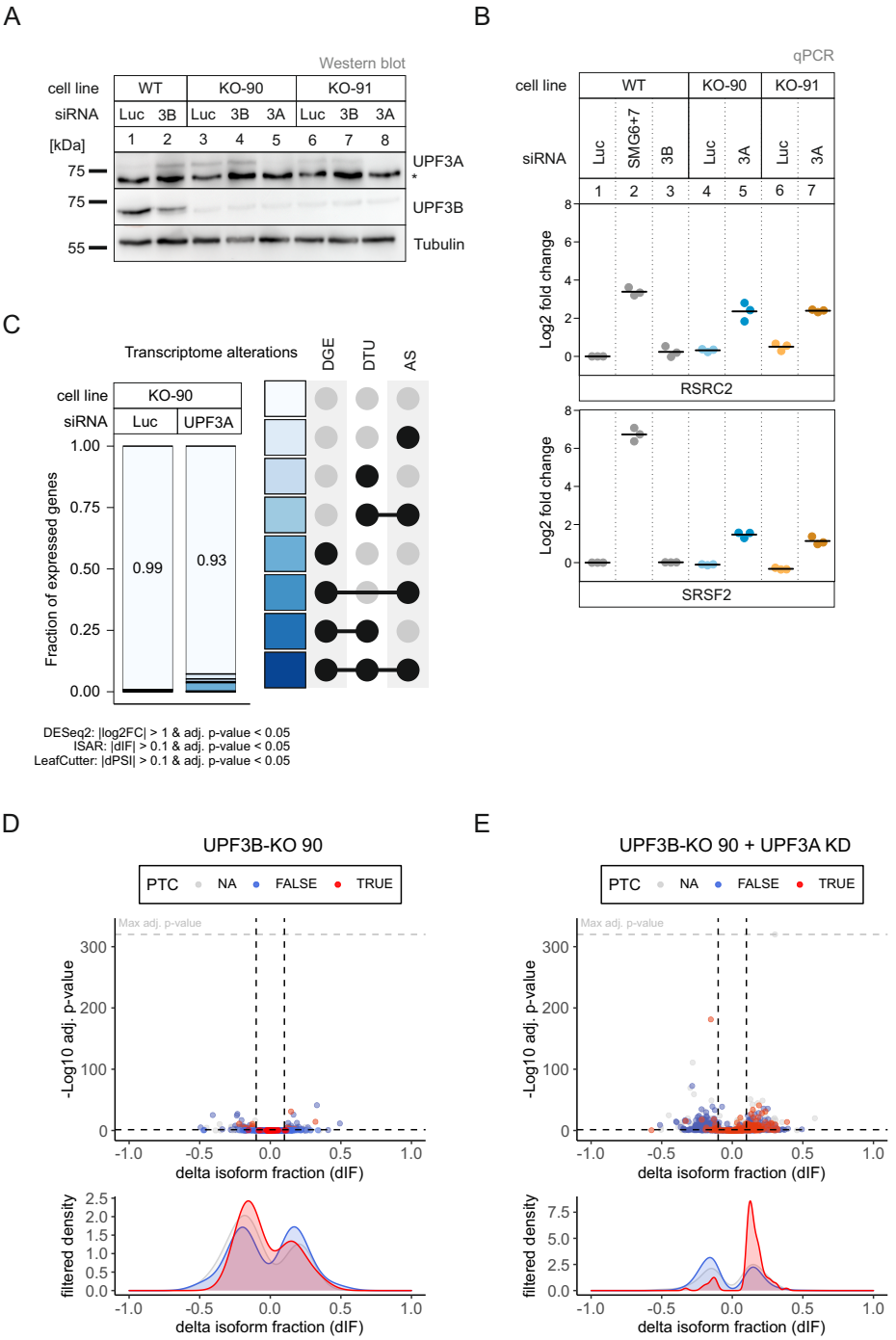

Figure 3 - Loss of UPF3B does not affect NMD efficiency, only in combination with KD of UPF3A

A Western blot analysis of WT and UPF3B KO cells (clones 90 and 91) combined with the indicated knockdowns. UPF3A and UPF3B (AK-141) protein levels were detected, Tubulin serves as control. The asterisk indicates unspecific bands.

B Quantitative RT-PCR of the indicated cell lines with the indicated knockdowns. For RSRC2 and SRSF2 the ratio of NMD isoform to canonical isoform was calculated. Data points and means are plotted as Log2 fold change (n=3).

C Fraction of expressed genes (genes with non-zero counts in DESeq2) were calculated which exhibit individual or combinations of differential gene expression (DGE), differential transcript usage (DTU) and/or alternative splicing (AS) events in the indicated conditions using the respective computational analysis (cutoffs are indicated). AS and DTU events were collapsed on the gene level. For DGE, p-values were calculated by DESeq2 using a two-sided Wald test and corrected for multiple testing using the Benjamini-Hochberg method. For DTU, p-values were calculated by IsoformSwitchAnalyzeR using a DEXSeq-based test and corrected for multiple testing using the Benjamini-Hochberg method. For AS, p-values were calculated by LeafCutter using an asymptotic Chi-squared distribution and corrected for multiple testing using the Benjamini-Hochberg method.

D,E Volcano plots showing the differential transcript usage (via IsoformSwitchAnalyzeR) in various RNA-Seq data. Isoforms containing GENCODE (release 33) annotated PTC (red, TRUE), regular stop codons (blue, FALSE) or having no annotated open reading frame (grey, NA) are indicated. The change in isoform fraction (dIF) is plotted against the -log10 adjusted p-value (adj.p-value). Density plots show the distribution of filtered isoforms in respect to the dIF, cutoffs were |dIF| > 0.1 and adj. p-value < 0.05. P-values were calculated by IsoformSwitchAnalyzeR using a DEXSeq-based test and corrected for multiple testing using the Benjamini-Hochberg method.

216 To gain more transcriptome-wide information, we performed RNA-seq of the UPF3B KO clone
217 90, with and without UPF3A siRNA treatment (Fig EV3C and Datasets EV1-EV3). The global
218 effects detected in the RNA-seq data correlated well with the NMD inhibition seen for single
219 targets (Figs 3C and EV3D-G). Analysis of the differential transcript usage revealed an
220 upregulation of transcripts annotated with a PTC only in the UPF3B KO cells with additionally
221 downregulated UPF3A (Figs 3D and E). This increase of NMD-sensitive transcripts could not
222 be observed in the plain UPF3B KO cells with UPF3A naturally upregulated. All together this
223 data strongly suggested at least partial redundancy of UPF3A and UPF3B, since KO of only
224 one paralog was irrelevant for NMD functionality. Furthermore, we were able to show that also
225 in the absence of UPF3B an overexpression of UPF3A has no negative effects on NMD
226 efficiency, supporting the previous conclusion of UPF3A not being a negative NMD regulator
227 (Figs EV3H and I).

228 **Stronger NMD impairment in UPF3A-UPF3B double KO cells**

229 Considering that UPF3A and UPF3B seemingly carry out redundant functions, we decided to
230 create a cell line completely lacking both paralogs and aimed to generate UPF3A-UPF3B
231 double KO cells (UPF3 dKO). These cells should show stronger effects than the combination
232 of a KO and a KD, since residual amounts of protein were typically still detected after siRNA
233 treatment. Using the UPF3B-KO clone 90 as parental cell line, two potential UPF3 dKO clones
234 1 and 2 were generated (Fig 4A), which differed in the guide RNAs used to target exon 1 of
235 UPF3A. We confirmed that both cell lines contained frame shift-inducing insertions/deletions
236 at the respective positions in the UPF3A gene (Figs 4B, EV4A and B). We first explored by
237 qPCR how strongly the dKO affected NMD (Fig 4C). For all three tested genes, the expression
238 of the NMD-sensitive isoform was further increased compared to the previously used
239 combination of UPF3B KO with additional UPF3A KD. Of note, the NMD inhibitory effect
240 observed in the dKOs became more pronounced after UPF3B siRNA transfection, suggesting
241 that low levels of residual UPF3B protein were still present in the dKO cells (Fig EV4C).

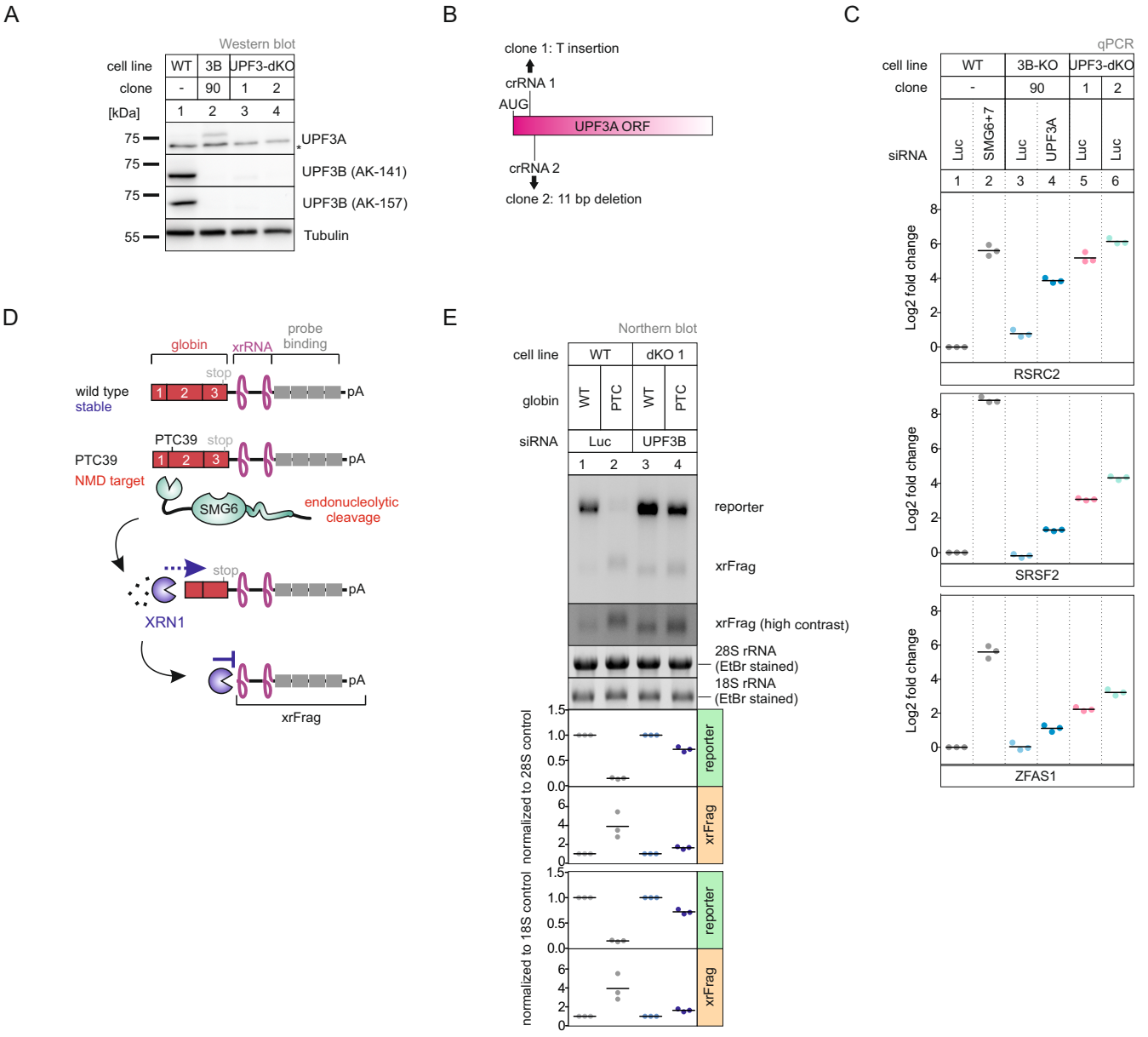

Figure 4 - KO of both UPF3 paralogs results in strongly impaired NMD
A Western blot analysis of WT, UPF3B KO and UPF3A-UPF3B doubleKO cells (clones 1 and 2). UPF3A and UPF3B protein levels were detected, Tubulin serves as control. The asterisk indicates unspecific bands.
B Schematic depiction of the insertion/deletion in the UPF3A open reading frame resulting in the additional UPF3A KO in the UPF3B KO clone 90 generating UPF3 dKO clones.
C Quantitative RT-PCR of the indicated samples with the indicated KDs. For RSRC2 and SRSF2 the ratio of NMD isoform to canonical isoform was calculated. ZFAS1 expression was normalized to C1orf43 reference. Data points and means are plotted as Log2 fold change (n=3).
D Schematic overview of the globin reporter constructs and their functional elements.
E Northern blot analysis of globin reporter and xrFrag. Ethidium bromide stained 28S and 18S rRNAs are shown as controls. Quantification results are shown as data points and mean (n=3).

243 The expression levels of endogenous NMD substrates could be influenced by transcription
244 rates or other indirect effects, which could lead to over- or underestimating NMD inhibition.
245 Therefore, we investigated the NMD efficiency in the dKO cells using the well-established β-
246 globin NMD reporter. To this end, we stably integrated β-globin WT or PTC39 constructs in
247 WT and UPF3 dKO cells (Fig 4D). These reporters also contained XRN1-resistant sequences
248 (xrRNAs) in their 3' UTRs, which allowed us to analyze not only the degradation of the full-
249 length reporter mRNA but also to quantify decay intermediates (called xrFrag) (Boehm *et al.*,
250 2016; Voigt *et al.*, 2019). The PTC39 mRNA was efficiently degraded and a strong xrFrag
251 observed in WT cells, whereas in dKO cells the PTC39 reporter accumulated to high levels
252 (72% compared to the WT mRNA), which was accompanied by a decrease in the amount of
253 xrFrag. (Fig 4E, lane 2 vs. lane 4). In line with the previous observations, this result indicated
254 a strong decrease of NMD activity upon the KO of both UPF3 paralogs using a robust NMD
255 reporter pair expressed independently of endogenous NMD substrates, supporting the
256 functional redundancy of UPF3A and UPF3B in NMD.

257 To establish transcriptome-wide insights into UPF3A and UPF3B function, we carried out RNA-
258 seq for both dKO clones, which was combined with and without UPF3B KD treatment to
259 eliminate as many of the potentially present remaining UPF3B proteins (Fig EV5A and
260 Datasets EV1-EV3). Differential gene expression analysis showed that more than three times
261 as many genes were upregulated than downregulated in both dKO cells (Figs 5A and EV5B).
262 This is consistent with the redundant role of UPF3B and UPF3A as supporting NMD factors.
263 The considerable overlap between both clones also suggests that we identified high-
264 confidence UPF3 targets. Furthermore, 1072 of these gene were also significantly upregulated
265 in previously generated SMG7 KO plus SMG6 KD data (Fig EV5C, ref data: (Boehm *et al.*,
266 2021)) indicating that these are universal NMD-targets and not specific to a certain branch of
267 the NMD pathway. In addition to DGE, subsets of the expressed genes showed changes in
268 alternative splicing or/and differential transcript usage (Fig 5B). In total, 14-16 % of the global
269 transcriptome showed single or combined changes (DGE, DTU and/or AS) and up to 20%
270 when the cells were treated with an additional UPF3B KD.

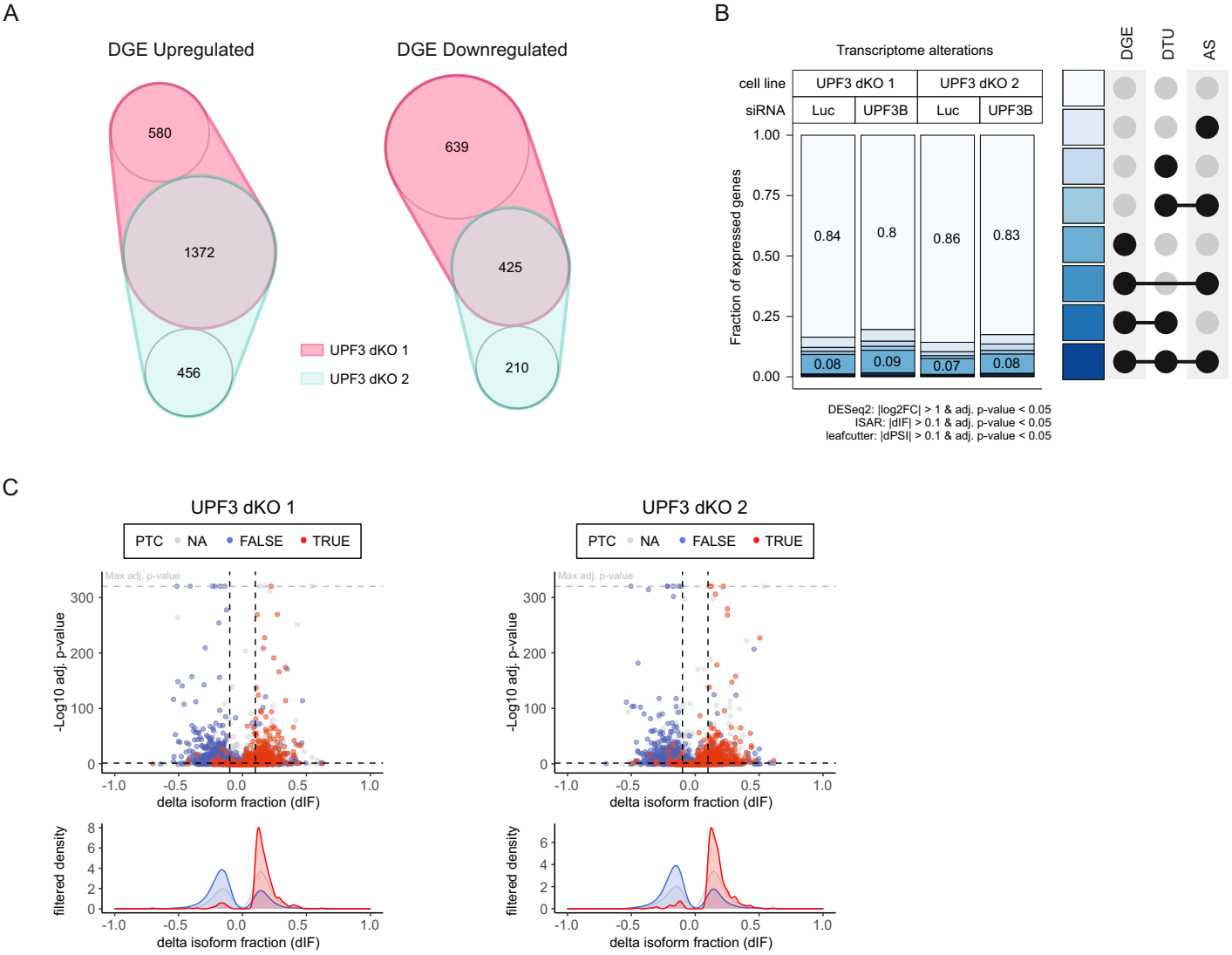

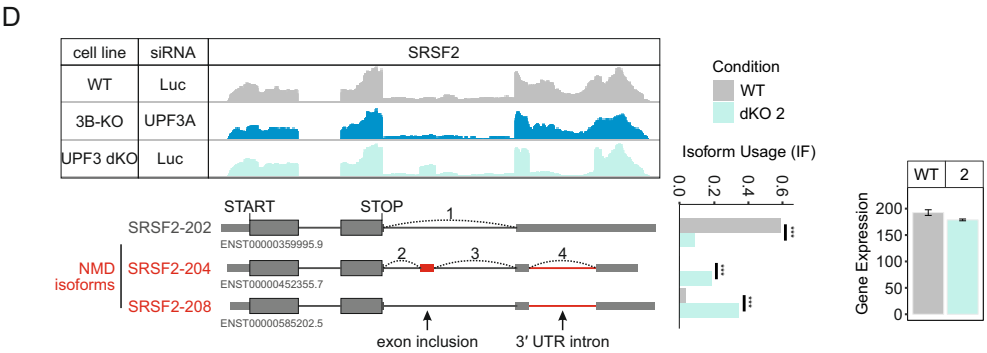

Figure 5 - RNA-seq reveals strong global upregulation of NMD-sensitive targets upon UPF3 dKO in HEK293 cells

A nVenn Diagram showing the overlap of up- or downregulated genes in the UPF3 dKO cell lines 1 and 2. Log2 fold change <-1 (downregulated) or >1 (upregulated) and adjusted p-value (padj) < 0.05. DGE = Differential Gene Expression.

B Fraction of expressed genes (genes with non-zero counts in DESeq2) were calculated which exhibit individual or combinations of differential gene expression (DGE), differential transcript usage (DTU) and/or alternative splicing (AS) events in the indicated conditions using the respective computational analysis (cutoffs are indicated). AS and DTU events were collapsed on the gene level. For DGE, p-values were calculated by DESeq2 using a two-sided Wald test and corrected for multiple testing using the Benjamini-Hochberg method. For DTU, p-values were calculated by IsoformSwitchAnalyzeR using a DEXSeq-based test and corrected for multiple testing using the Benjamini-Hochberg method. For AS, p-values were calculated by LeafCutter using an asymptotic Chi-squared distribution and corrected for multiple testing using the Benjamini-Hochberg method.

C Volcano plots showing the differential transcript usage (via IsoformSwitchAnalyzeR) in various RNA-Seq data. Isoforms containing GENCODE (release 33) annotated PTC (red, TRUE), regular stop codons (blue, FALSE) or having no annotated open reading frame (grey, NA) are indicated. The change in isoform fraction (dIF) is plotted against the -log10 adjusted p-value (adj.p-value). Density plots show the distribution of filtered isoforms in respect to the dIF, cutoffs were |dIF| > 0.1 and adj.p-value < 0.05. P-values were calculated by IsoformSwitchAnalyzeR using a DEXSeq-based test and corrected for multiple testing using the Benjamini-Hochberg method.

D Read coverage of SRSF2 from the indicated RNA-seq sample data with or without UPF3A siRNA treatment shown as Integrative Genomics Viewer (IGV) snapshot. The canonical and NMD-sensitive isoforms are schematically indicated below. Quantification of isoforms by IsoformSwitchAnalyzeR (right).

272 In agreement with NMD inhibition in the dKOs, we saw that many transcripts containing a PTC
273 were up-regulated, while the corresponding transcripts without a PTC were down-regulated.
274 (Figs 5C and EV5D). Under these conditions, the IGV snapshot of the NMD-target SRSF2
275 showed NMD-inducing exon inclusion and 3' UTR splicing events, which were not visible in
276 combined UPF3B KO/UPF3A KD cells (Fig 5D). Collectively, the RNA-seq data support the
277 previously observed strong NMD inhibition in response to the complete absence of both UPF3
278 paralogs and hence their proposed redundancy.

279 **UPF3A supports NMD independent of a bridge function**

280 Next, we aimed to analyze whether the severe effects in the dKOs are at least partly due to
281 the loss of a protein-protein interaction bridge between UPF2 and the EJC, while the presence
282 of UPF3A in the UPF3B KOs preserved this function ensuring NMD functionality. Therefore,
283 we expressed FLAG-tagged UPF2 in WT, UPF3B KO and UPF3A-UPF3B dKO cells and
284 analyzed the UPF2 interactome using mass spectrometry (Dataset EV4). Consistent with the
285 previously described interaction partners, we found many NMD factors as well as EJC proteins
286 in the UPF2 interactome in WT cells (Fig 6A). Contrary to our expectation, the three EJC core
287 components (EIF4A3, RBM8A, MAGOHB) barely co-precipitated with UPF2 in the absence of
288 UPF3B (compared to control: log2 FC = 0.58, 0.63 and 0.74, respectively; Fig 6B) and were
289 therefore strongly decreased in comparison to the WT cells (Fig EV6A). Hence, the UPF2-
290 bound UPF3A was unable to establish a stable interaction with the EJC. Surprisingly, in the
291 UPF3B KO cells the EJC-associated CASC3 still showed relatively high levels of co-
292 precipitation (log2 FC = 4.42), which therefore appears to be independent of the interaction
293 with the other EJC components. In the dKOs all interactions with EJC proteins including
294 CASC3 were completely lost (Figs 6C and EV6B). The latter was also observed in a
295 comparable approach employing stable isotope labeling with amino acids in cell culture
296 (SILAC) to analyze the UPF2 interactome in the WT and dKO cells (Dataset EV5). All EJC
297 core components that were highly co-precipitated in WT cells were lost in the absence of both
298 UPF3 paralogs (Figs EV6C-E).

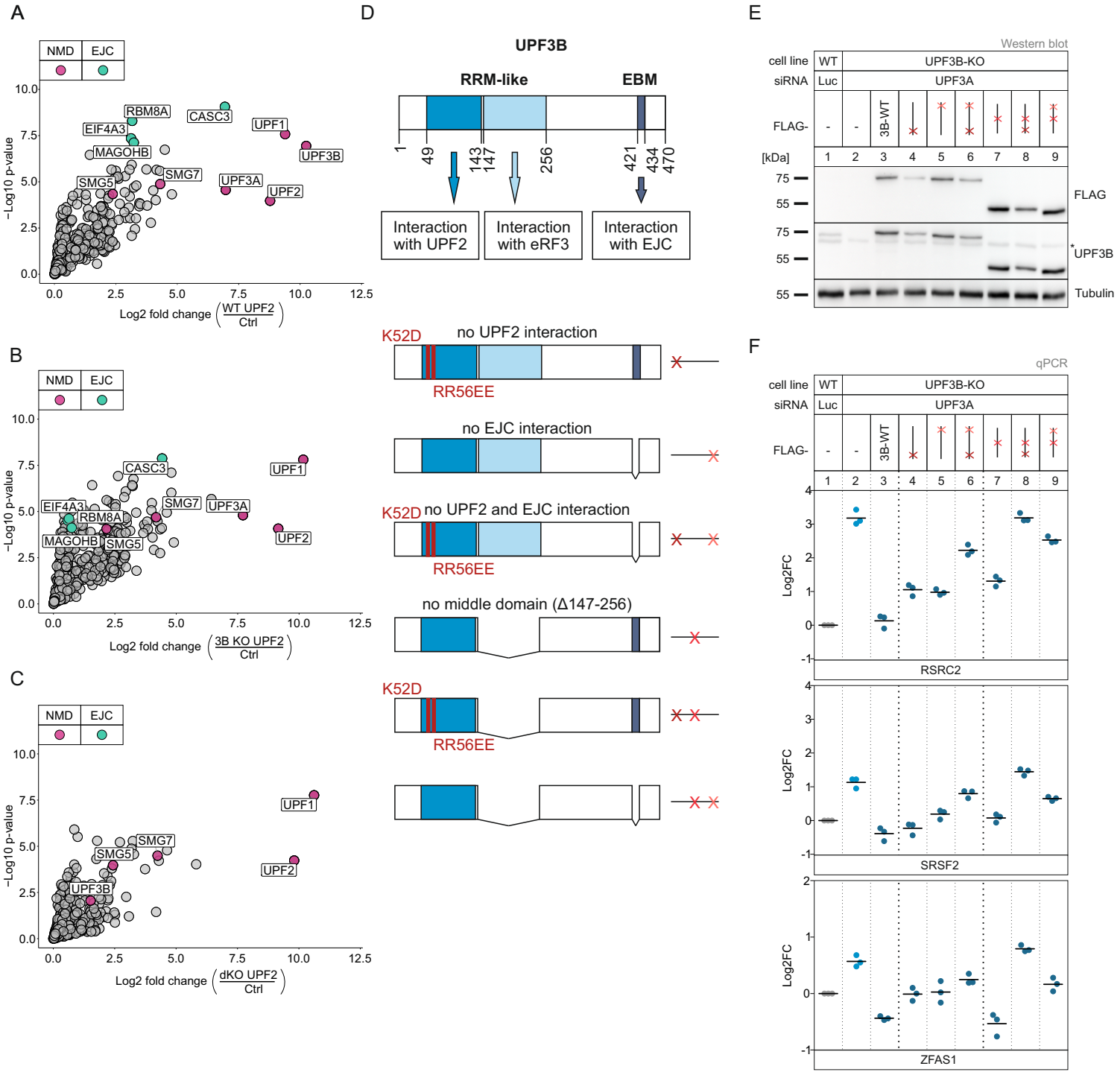

Figure 6 - Interaction of UPF3A and UPF3B with the EJC is dispensable to elicit NMD

A-C Volcano plots of label free mass spectrometry-based analysis of the interaction partners of UPF2 in WT cells treated with control siRNAs and the UPF3B KO clone 90 and dKO clone 1 both treated with siRNAs targeting UPF3B (n = 4 biologically independent samples). (A) FLAG-UPF2 in WT against FLAG-GST control in WT cells, (B) UPF2 in 3B KO cells against FLAG control in WT cells, (C) UPF2 in dKO cells against FLAG control in WT cells. Points labeled in purple indicate NMD factors; points labeled in turquoise indicate EJC components. Cut offs: Log2 fold change ≥ 0

D Schematic representation of the UPF3B protein domains and the respective functions. Below are the mutated rescue constructs and their respective abstract placeholders.

E Western blot analysis of WT and UPF3B KO clone 90 with Luciferase and UPF3A KDs respectively. Monitored expression of the FLAG-tagged UPF3B rescue construct shown in (D). Rescue construct protein levels were detected with anti-FLAG and anti-UPF3B (AK-141) antibodies. Tubulin serves as control. The asterisk indicates unspecific bands.

F Quantitative RT-PCR of the samples from (E). For RSRC2 and SRSF2 the ratio of NMD isoform to canonical isoform was calculated. ZFAS1 expression was normalized to C1orf43 reference. Data points and means are plotted as log2 fold change (n=3).

300 **Partially redundant functions of UPF3B domains are required for NMD**

301 With regard to the surprising observation that UPF3A apparently elicits NMD without
302 interacting with the EJC, we aimed to investigate the molecular features required by UPF3 to
303 support NMD via rescue experiments. In principle, the UPF3 dKO cells represent an ideal
304 system for this approach. However, apart from the residual amounts of UPF3B that were still
305 expressed, we noticed that the UFP3 dKOs were able to upregulate the expression of a
306 shortened UPF3B variant after long-term cultivation.

307 Since this phenomenon did not occur in the single UPF3B KOs, we generated stable UPF3B
308 KO cell lines expressing various inducible UPF3B constructs with individual or combined
309 binding site mutations (Figs 6D and E and EV6F). Transfection of these cells with UPF3A
310 siRNAs resulted in the robust depletion of UPF3 for the analysis of the rescue activities of
311 individual UPF3B variants. Considering the established role of UPF3B as a bridge between
312 UPF2 and the EJC, which we validated in the mass spec analysis, it was surprising to see that
313 disruption of either of these interactions did not affect or only mildly affected UPF3B's rescue
314 capacity, depending on the analyzed NMD substrate (Fig 6F, lane 3 vs. lanes 4 and 5). This is
315 partially consistent with the observed functional NMD in UPF3B KOs, despite the apparent
316 inability of UPF3A to form a bridge between UPF2 and the EJC (Figs 3C and 6B). However,
317 mutating both UPF3B binding sites (disrupting UPF2 and EJC binding) largely inactivated the
318 NMD-related function of UPF3B.

319 It was recently reported that EJC-bound or free UPF3B can interact with the eukaryotic release
320 factor 3 (eRF3) via the so far uncharacterized middle domain (aa 147-256) (Neu-Yilik *et al.*,
321 2017). With this interaction and binding of the terminating ribosome, UPF3B can delay
322 translation termination, which defines aberrant termination events and triggers NMD (Amrani
323 *et al.*, 2004; Neu-Yilik *et al.*, 2017; Peixeiro *et al.*, 2012). To investigate the impact of this
324 interaction on NMD, we created UPF3B variants lacking that specific middle domain or
325 combined the deletion with the previously used interaction mutations (Fig 6D and E). We
326 observed a similar pattern as the UPF3B mutants examined in the previous experiment: when

327 only the middle domain was deleted, UPF3B was able to rescue NMD comparable to the WT
328 protein or slightly worse (Fig 6F lane 7). In combination with a mutation in the UPF2- or the
329 EJC binding site its function in NMD was severely impaired (lanes 8 and 9). This suggests that
330 if the classic bridge formation is inhibited by removing either of the interaction sites, UPF3B
331 relied on the function carried out by the uncharacterized middle domain.

332 As further support for the NMD promoting effect of UPF3A on NMD, we performed a rescue
333 experiment in the above used UPF3B KO UPF3A KD cells (Figs 7A and B). Expression of the
334 siRNA insensitive UPF3A construct restored NMD functionality with similar efficiency as the
335 UPF3B rescue (Fig 7C lane 3 vs. lane 5), underlining our previous statement: UPF3A supports
336 and elicits NMD comparably to its paralog UPF3B.

337 Also comparable to UPF3B, UPF3A has a second naturally occurring isoform but instead of
338 skipping exon 8 (like UPF3B) it excludes its fourth exon. This isoform is transcribed in
339 approximately one third of the cases (Fig EV6G) in WT HEK293 cells but cannot be detected
340 on protein levels. We were interested, whether this isoform was as potent to elicit NMD as the
341 full-length construct. Expression of the exon 4 UPF3A deletion construct in the UPF3 depleted
342 cells showed no rescue (Fig 7C lane 4). Hence, exon 4 must encode for an essential region
343 required for the bridge-independent function of UPF3A.

344 In view of these observations and the close proximity of exon 4 (124-157) to the middle domain
345 (147-256), we decided to investigate which effect the deletion of the homologous exon 4 in the
346 paralog UPF3B has. The UPF3B Δe4 construct behaved like the corresponding UPF3A
347 construct and showed no NMD rescue activity (lane 6). However, the expression of the N-
348 terminus of UPF3B was able to restore NMD comparably to the WT protein (lane 7). This is
349 consistent with all our previous findings, since the first 279 amino acids contain the UPF2
350 binding site as well as the middle domain, which was shown to be sufficient to elicit NMD (Fig
351 6F lane 5). Due to the fact that the C-terminus contains only one interaction site and lacks exon
352 4, its incapability to rescue NMD is in line with our previous experiments. Overall, our results

353 identify exon 4 of UPF3 as a previously unnoticed region that is essential for its function in
354 NMD.
355

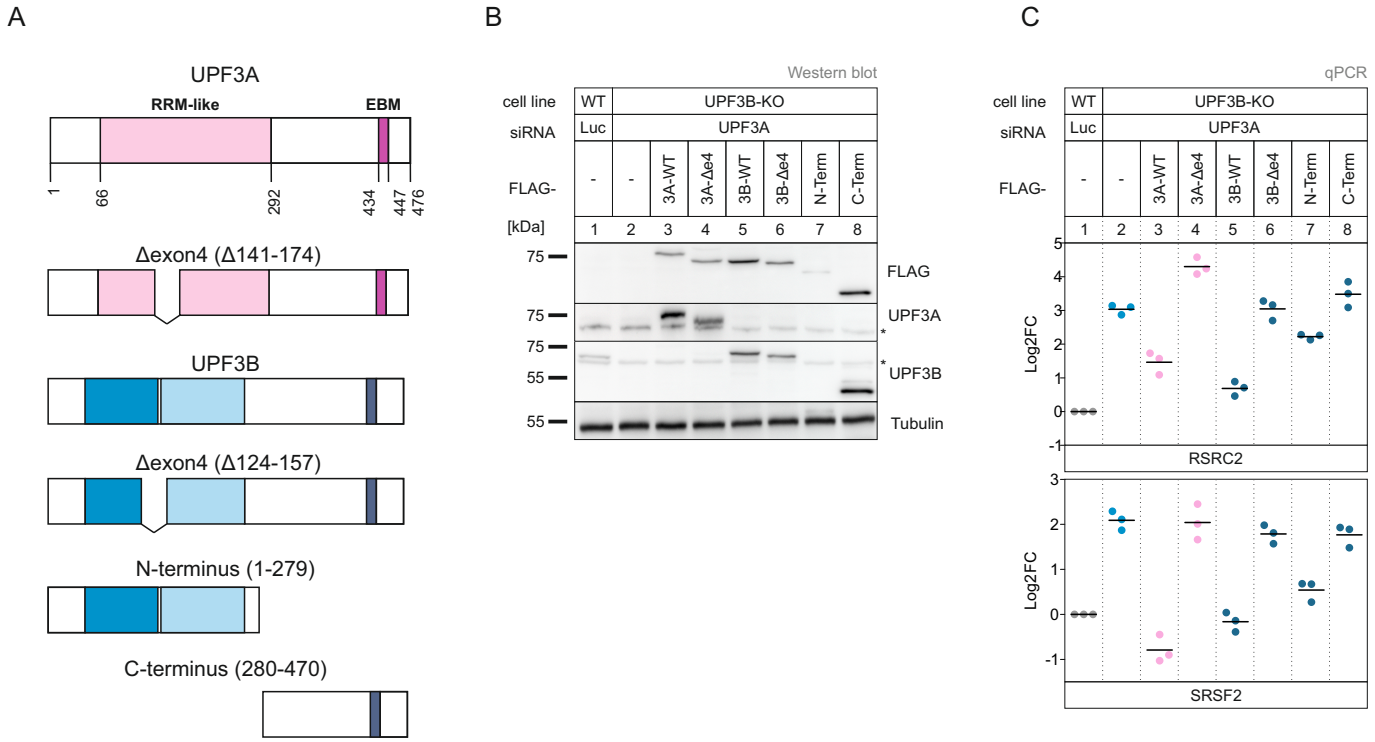

Figure 7 - WT UPF3A can rescue NMD in full extent. Deletion on exon 4 disrupts functionality in both paralogs.
A Schematic representation of the UPF3A and UPF3B protein domains. Below are the respective mutated rescue constructs.
B Western blot analysis of WT and UPF3B KO clone 90 with Luciferase and UPF3A KDs respectively. Monitored expression of the FLAG-tagged UPF3A and UPF3B rescue construct shown in (A). Rescue construct protein levels were detected with anti-FLAG, anti-UPF3A and anti-UPF3B (AK-141) antibodies. Tubulin serves as control. The asterisk indicates unspecific bands.
C Quantitative RT-PCR of the samples from (B). For RSRC2 and SRSF2 the ratio of NMD isoform to canonical isoform was calculated. Data points and means are plotted as log2 fold change (n=3).

358 **Discussion**

359 Methodological advances - be it improved analytics or novel experimental approaches - can
360 help to find new answers to old biological problems. Equipped with powerful new molecular
361 biology methods, we set out to answer the question which functions the two UPF3 paralogs
362 carry out in human cells. Since the initial description of mammalian UPF3A and UPF3B (Lykke-
363 Andersen *et al.*, 2000; Serin *et al.*, 2001), many researchers have been engaged in determining
364 the function and work distribution of these two proteins in NMD. It became clear relatively early
365 that UPF3A and UPF3B can both interact with UPF2 as well as the EJC and activate NMD
366 (Gehring *et al.*, 2003; Kim *et al.*, 2001; Lykke-Andersen *et al.*, 2000; Serin *et al.*, 2001). But
367 significant differences in these interactions and the amounts of UPF3A and UPF3B proteins
368 were also found, leading to the hypothesis that UPF3B is the central player and UPF3A more
369 its backup (Chan *et al.*, 2009; Kunz *et al.*, 2006). The investigations were further intensified
370 upon the discovery that mutations in the human UPF3B gene lead to various forms of mental
371 disorder (Nguyen *et al.*, 2014). Disease severity seems to be dictated by the amount of UPF3A
372 present, suggesting again a compensatory mechanism and redundant functions of UPF3B and
373 UPF3A (Nguyen *et al.*, 2012).

374 Later, it was reported that in mouse cells UPF3B is an NMD activator and UPF3A is an NMD
375 inhibitor (Shum *et al.*, 2016). Accordingly, removal of UPF3A resulted in enhanced NMD,
376 whereas removal of UPF3B inhibited NMD. Recently, another function of UPF3B was
377 discovered, namely that it is involved in different phases of translation termination (Neu-Yilik
378 *et al.*, 2017). UPF3B not only interacts with release factors, but also slows down translation
379 termination and promotes dissociation of post-termination ribosomal complexes. Whether
380 these functions of UPF3B in translation termination are related to its function in NMD has not
381 been clarified to date.

382 Although our results cannot fully answer this last question, we have more or less definite
383 answers for the functions of the two proteins UPF3A and UPF3B in NMD. All our data support
384 the notion that the presence of UPF3B or UPF3A is sufficient to maintain NMD activity in

385 human cells. First, we see at most a weak inhibition of NMD in our HEK293 UPF3B KO cells.
386 However, this does not necessarily mean that all cell types display full NMD activity after a KO
387 of UPF3B. Instead, it is conceivable that HEK293 cells are just particularly robust against the
388 UPF3B depletion or particularly efficient at the compensatory upregulation of UPF3A. Likewise,
389 we see no NMD inhibition in cells overexpressing UPF3A or NMD "boosting" in UPF3A KO
390 cells. Only when we deplete in UPF3A or UPF3B KO cell lines the respective other protein by
391 RNAi or genomic KO, NMD efficiency substantially decreases. It should be noted that the
392 effects of a KO on NMD activity are typically stronger than those of a KD, which is consistent
393 with our earlier observations (Boehm *et al.*, 2021; Gerbracht *et al.*, 2020). Although our data
394 clearly argue against an NMD-inhibitory function of UPF3A, experimental differences exist
395 between our work and the work describing the NMD inhibition by UPF3A. While we have used
396 human HEK293 cells, the results of Shum et al. were obtained in P19 mouse cells and mouse
397 embryonic fibroblasts (MEFs). Both, the different organisms and the different types of cells
398 could have influenced the results. Interestingly, in a parallel manuscript, Yi et al. find that
399 mouse UPF3A can rescue NMD in human HCT116 UPF3A-UPF3B dKO cells (Yi *et al.*, 2021).
400 Although these results were obtained in a heterologous context, mouse UPF3A does not
401 appear to be a general NMD inhibitor.

402 The different KO cells that we have generated in the course of this project enabled us to
403 conduct experiments that went beyond investigating UPF3-dependent NMD substrates in
404 human cells. Specifically, we were able to study the composition of NMD complexes without
405 UPF3B or both UPF3 proteins and to carry out rescue experiments with different UPF3A and
406 UPF3B protein variants. Not entirely unexpected, we observed that in the absence of UPF3A
407 and UPF3B, the interaction between UPF2 and the EJC is lost. This bridging by UPF3 between
408 UPF2-containing NMD complexes and the EJC was previously considered to be essential for
409 NMD. However, two observations argue against UPF3 being mainly a bridging protein. First,
410 UPF3B mutants that cannot interact with either the EJC or UPF2 fully rescue NMD. Only when
411 both interaction sites were mutated, UPF3 lost its NMD function. This indicates that the
412 interaction with one of the two interaction partners is sufficient to maintain NMD. Second, we

413 observed that not only in UPF3 double-KO cells, but also in UPF3B KO cells, the bridge
414 between UPF2 and the EJC was lost. Although quite surprising at first glance, this is in good
415 agreement with previous results showing that the interaction between the EJC and UPF3A is
416 substantially weaker than that between the EJC and UPF3B (Kunz *et al.*, 2006). Indeed, earlier
417 structural data also argue against a bridging function of UPF3. In the cryo-EM structure of an
418 EJC-UPF3-UPF2-UPF1 complex, UPF1 did not face towards a possible terminating ribosome
419 in the 5' direction, but instead in 3' direction (Melero *et al.*, 2012). Therefore, one could
420 conclude that the interactions between all these proteins do not take place at a single time
421 point during NMD.

422 This raises the question of what UPF3 function is essential for NMD, if it is not its bridging
423 function? Our rescue experiments showed that the middle domain of UPF3B cooperates with
424 the UPF2- and the EJC interaction sites, i.e., its deletion in combination with one other mutation
425 inactivates UPF3B. The middle domain has been described to mediate the interaction of
426 UPF3B with release factor 3 (RF3), but this interaction has not been demonstrated for UPF3A
427 (Neu-Yilik *et al.*, 2017). So, if UPF3A cannot interact with RF3 and also binds weaker to the
428 EJC as noted above, it should be functionally inactive. However, we see no obvious difference
429 between UPF3B and UPF3A in the rescue experiments. These and other observations can, in
430 our view, only be explained with more complex models, which must also consider non-linear
431 relationships and potential auxiliary functions of certain regions of UPF3 (Fig 8).

432 Since the interactions of UPF3 are essential only in combination with each other, we propose
433 that UPF3A and UPF3B exert multiple functions at different time points of NMD and in
434 association with different complexes. We only consider here the previously described
435 interactions of UPF3 with UPF2, the EJC and the release factor 3 (Fig 8B). While it was
436 previously described that UPF3B interacts better than UPF3A with UPF2 (Chan *et al.*, 2009),
437 we find both proteins in the FLAG-UPF2 IP. The amount of UPF3A does not seem to increase
438 when UPF3B is depleted, which could be due to the overexpression of UPF2 in our
439 experimental system. The interaction of UPF3 and UPF2 is also conserved in yeast and is thus

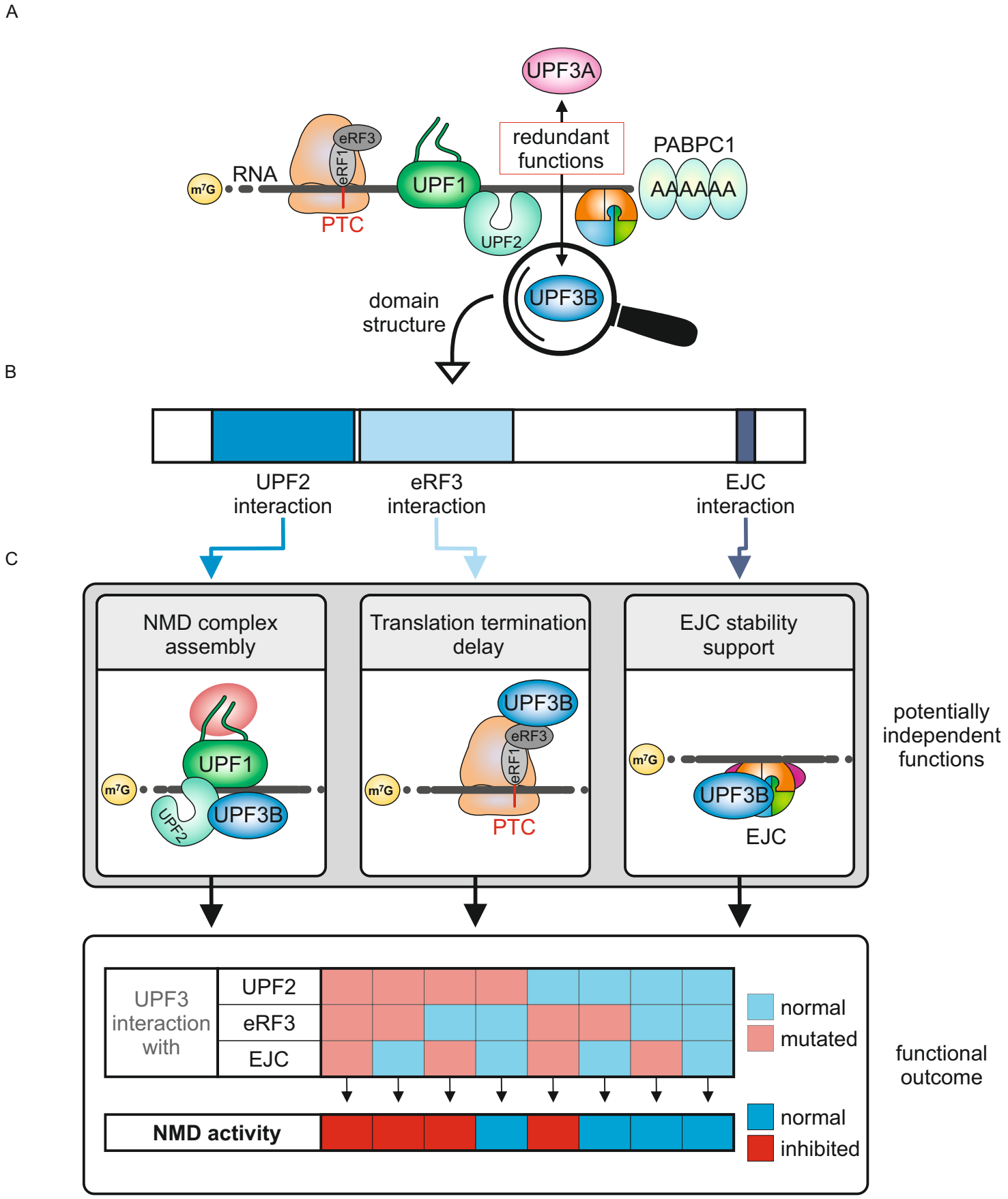

Figure 8 - Model for potentially independent functions of UPF3 in NMD.
A Both UPF3 paralogs UPF3A and UPF3B can elicit NMD and trigger mRNA degradation. We propose a new model where UPF3B exerts multiple functions at different timepoints during NMD.
B Schematic overview of UPF3B domain structure and the postulated functions.
C Via the RRM-like domain in the N-terminus of the protein it interacts with UPF2, which might be important for the assembly of an NMD-inducing complex. The middle domain was ascribed to be responsible for the interaction with eRF3 and potential translation termination delay. The interaction with the EJC via the EBM could stabilize the complex by preventing its interaction with the disassembly factor PYM1. Only if two out of the three functions are ensured, NMD can pursue and degrade the targeted mRNA.

441 likely to have functional significance. However, a UPF3B mutant in which binding to UPF2 was
442 inactivated rescues NMD better than the UPF3B WT.

443 The interaction of the middle domain of UPF3B with RF3 has only recently been described
444 (Neu-Yilik *et al.*, 2017). Again, we find that removing only the middle domain does not
445 substantially inhibit NMD. In combination with an inactivation of the UPF2 binding, the deletion
446 of the middle domain leads to a complete inhibition of the NMD in the rescue assay. This could
447 also happen when exon 4 of UPF3B or UPF3A is removed, which is located at the junction
448 between the UPF2 binding domain and the middle domain. Therefore, UPF3A Δexon4 would
449 be a naturally occurring, NMD-inactive variant of the UPF3 proteins.

450 How might the different regions and domains communicate with each other and regulate the
451 function of UPF3 in NMD? The function of the middle domain in relation to NMD has not yet
452 been investigated. It is conceivable that UPF3B plays a minor role in translation termination
453 and that the events that trigger NMD can also occur without the middle domain - potentially
454 with a delay (Figure 8c). Therefore, the deletion of the middle domain could be tolerated in
455 isolation but would become fatal in combination with other mutations that impair additional
456 functions. With regard to the EBM, we propose that its binding stabilizes the EJC, for example
457 by preventing the interaction of the EJC with PYM1 (Fig 8C). PYM1 is a known EJC
458 disassembly factor and binds to the EJC at a surface area that overlaps with the EBM binding
459 site (Bono *et al.*, 2004; Buchwald *et al.*, 2010; Gehring *et al.*, 2009). We suggest that in cells
460 rescued with the ΔEBM mutant EJCs are more readily dissociated from the mRNA in the
461 cytoplasm. The concomitant loss of UPF3B's termination function (Δmiddle domain, ΔEBM)
462 would have a dramatic effect on NMD efficiency, because NMD would be initiated too slowly.
463 Likewise, the interaction of UPF3 with UPF2 might be important for the assembly of an NMD-
464 inducing complex (Fig 8C) that needs to be timed with translation termination and that leads
465 to NMD activation only in the presence of the EJC. Although these suggestions may not
466 accurately reflect the molecular events during NMD, they illustrate possible functions of the
467 domains of UPF3, particularly in relation to their NMD-inactive combinations (Fig 8). Overall,

468 our observations fit well with a "synthetic lethal" model in which inactivation of any two domains
469 together disrupts UPF3 activity.

470 One factor whose function needs to be examined in more detail in the context of UPF3 is
471 CASC3. Our mass spectrometry analysis shows that CASC3 immunoprecipitates very well
472 with UPF2 in wildtype cells. CASC3 still partially precipitates with UPF2 in UPF3B KO cells,
473 although the interaction of the other EJC factors is reduced to background levels. In previous
474 work, we observed that UPF3B interacts less well with the EJC when CASC3 is knocked out
475 (Gerbracht *et al.*, 2020). This indicates that an interaction between CASC3 and the UPF3
476 proteins exists that is not well understood so far. What kind of interaction this is and what
477 function it has will be interesting to address in future experiments.

478 Our own work and the work of Yi et al. have re-examined the functions of the human UPF3
479 paralogues UPF3A and UPF3B (Yi *et al.*, 2021). Together, the studies confirmed some
480 previous findings and disconfirmed others, thereby successfully (re-)defining the role of UPF3
481 proteins in human cells. A few questions remain unanswered and need to be addressed in the
482 future, for example how exactly the middle domain supports NMD. As described above, our
483 results have implications for the understanding of the NMD mechanism, as they are
484 incompatible with, and thus exclude, certain models of NMD. In addition, they may also help
485 to better understand the link between UPF3B and intellectual disability and which domains of
486 UPF3A modulate the severity of the disease and may therefore be potential targets for therapy.

487

488

489 # Materials and Methods

490 ## Cell Culture

491 Flp-In T-Rex 293 (human, female, embryonic kidney, epithelial; Thermo Fisher Scientific,
492 RRID:CVCL_U427) cells were cultured in high-glucose, GlutaMAX DMEM (Gibco)
493 supplemented with 9% fetal bovine serum (Gibco) and 1x Penicillin Streptomycin (Gibco). The
494 cells were cultivated at 37°C and 5% CO_2 in a humidified incubator. The generation of knockout
495 and stable cell lines is described below and all cell lines are summarized in Dataset EV6.

496 ## siRNA-mediated knockdowns

497 For reverse transfection the cells were seeded at a density of 2.5 x 10^5 cells per well. The
498 transfection solution contained 2.5 µl Lipofectamine RNAiMAX and 60 pmol of the respective
499 siRNAs. For the UPF3A and UPF3B knockdowns 30 pmol of both belonging siRNAs were
500 used. In preparation for mass spectrometry, 2.5 x 10^6 were reverse transfected in 10 cm plates
501 using 6.25 µl Lipofectamine RNAiMAX and 150-200 pmol siRNA (or half of it for each of the
502 two siRNAs for UPF3A or UPF3B). All siRNAs used in this study are listed in Dataset EV6.

503 ## Plasmid transfection

504 For each stable transfection 2.5-3.0 x 10^5 cells were seeded one day prior transfection in 6-
505 wells. To express the N-terminally FLAG-tagged protein constructs and reporter mRNAs for
506 northern blotting, they were stably integrated using the PiggyBac (PB) Transposon system with
507 the cumate-inducible PB-CuO-MCS-BGH-EF1-CymR-Puro vector. This vector was modified
508 from the original vector (PB-CuO-MCS-IRES-GFP-EF1α-CymR-Puro (System Biosciences))
509 by replacing the IRES-GFP cassette with a BGH polyA signal. Per well 1.0 µg of the respective
510 PB vector and 0.8 µg PB Transposase were transfected using a calcium phosphate-based
511 system with BES buffered saline (BBS). Additionally, 0.5 µg of pCI-maxGFP was transfected
512 as a visual feedback for transfection efficiency. 48 h later, the cells were pooled in 10 cm plates
513 and selected for positive cells by incubation in media containing 2 µg/ml puromycin for a week.
514 To induce expression of the constructs, 30 µg/ml cumate was added and the cells were
515 harvested after 72h for continuing experiments.

516 The mRNA reporter constructs β-globin WT and β-globin PTC are available on Addgene (IDs
517 108375-108376). All vectors used in this study are listed in Dataset EV6.

518 Generation of knockout cells using CRISPR-Cas9

519 The knockouts were performed using the Alt-R CRISPR-Cas9 system (Integrated DNA
520 Technologies) and reverse transfection of a Cas9:guideRNA ribonucleoprotein complex using
521 Lipofectamine RNAiMAX (Thermo Fisher Scientific) according to the manufacturer's protocol.
522 The crRNA sequence (Integrated DNA Technologies) to target UPF3B was
523 /AltR1/rArGrArUrArArGrCrArGrGrArUrCrGrCrArArCrArGrUrUrUrUrArGrArGrCrUrArUrGrCrU/
524 AltR2/. For UPF3A the crRNA sequences were /AltR1/rCrCrGrCrArArCrCrGrGrArGrGrArC
525 rGrArArGrUrGrUrUrUrUrArGrArGrCrUrArUrGrCrU/AltR2/ for clone 1 and /AltR1/rGrCrGrGr
526 UrGrGrArArCrUrGrCrArCrUrUrCrUrArGrUrUrUrUrArGrArGrCrUrArUrGrCrU/AltR2/ for clone
527 2. Reverse transfection was performed on 1.5×10^5 cells per crRNA in 12-well plates. 48 h after
528 transfection the cells were trypsinized, counted and seeded at a mean density of a single cell
529 per well in 96-well plates. Cell colonies originating from a single clone were then screened via
530 Western blot and genome editing of UPF3A and UPF3B was analyzed on the genomic level
531 via DNA extraction and Sanger sequencing. Alterations on the transcript level were analyzed
532 via RNA extraction followed by reverse transcription and Sanger sequencing.

533 DNA and RNA extraction

534 Genomic DNA extraction using QuickExtract DNA Extraction Solution (Lucigen) was
535 performed according to manufacturer's instruction. For RNA extraction cells were harvested
536 with 1 ml RNAsolv reagent (Omega Bio-Tek) per 6 well and RNA was isolated according to
537 manufacturer's instruction, with the following changes: instead of 200 µl chloroform, 150 µl 1-
538 Bromo-3-chloropropane (Sigma-Aldrich) was added to the RNAsolv. Additionally, in the last
539 step the RNA pellet was dissolved in 20 µl RNase-free water by incubating for 10 min on a
540 shaking 65 °C heat block.

541 **Western blotting**

542 SDS-polyacrylamide gel electrophoresis and immunoblot analysis were performed using
543 protein samples harvested with RIPA buffer (50 mM Tris/HCl pH 8.0, 0.1% SDS, 150 mM NaCl,
544 1% IGEPAL, 0.5% deoxycholate) or samples eluted from Anti-FLAG M2 magnetic beads. For
545 protein quantification, the Pierce Detergent Compatible Bradford Assay Reagent (Thermo
546 Fisher Scientific) was used. All antibodies used in this study are listed in Dataset EV6.
547 Detection was performed with Western Lightning Plus-ECL (PerkinElmer) or ECL Select
548 Western Blotting Detection Reagent (Amersham) and the Vilber Fusion FX6 Edge imaging
549 system (Vilber Lourmat).

550 **Semi-quantitative and quantitative reverse transcriptase (RT)-PCR**

551 Reverse transcription was performed with 1-4 µg of total RNA in a 20 µl reaction volume with
552 10 µM VNN-$(dT)_{20}$ primer and the GoScript Reverse Transcriptase (Promega). For the semi-
553 quantitative end-point PCRs the MyTaq Red Mix (Bioline) was used. Quantitative RT-PCRs
554 were performed with the GoTaq qPCR Master Mix (Promega), 2% of cDNA per reaction, and
555 the CFX96 Touch Real-Time PCR Detection System (Bio-Rad). Each biological replicate was
556 repeated in technical triplicates and the average Ct (threshold cycle) value was measured.
557 When isoform switches were measured, values for NMD sensitive isoforms were normalized
558 to the canonical isoforms to calculate ΔCt. For differentially expressed genes, the
559 housekeeping gene C1orf43 values were subtracted from the target value to receive the ΔCt.
560 To calculate the mean log2 fold changes three biologically independent experiments were
561 used. The log2 fold changes are visualized as single data points and mean. All primers used
562 in this study are listed in Dataset EV6.

563 **RNA-sequencing and computational analyses**

564 Four different RNA-seq experiments were performed: 1) unaltered Flp-In T-REx 293 wild type
565 (WT) cells and WT cells overexpressing the UPF3A WT construct via the PB-Transposase
566 system. 2) Flp-In T-REx 293 wild type (WT) cells transfected with Luciferase siRNA and the
567 UPF3A KO clones 14 and 20 treated with either Luciferase or UPF3B siRNAs. 3) The control

568 Flp-In T-REx 293 wild type (WT) cells with a Luciferase KD and the UPF3B KO clone 90
569 transfected with Luciferase or UPF3A siRNAs. 4) WT cells transfected with Luciferase siRNA
570 and the two UPF3 double KO cell lines 1 and 2 transfected with either Luciferase or UPF3B
571 siRNAs. RNA was purified using peqGOLD TriFast (VWR Peqlab; for UPF3B KO samples) or
572 the Direct-zol RNA MiniPrep kit including the recommended DNase I treatment (Zymo
573 Research; all other samples) according to manufacturer's instructions. Three biological
574 replicates were analyzed for each sample.

575 The Lexogen SIRV Set3 Spike-In Control Mix (SKU: 051.0x; for UPF3B KO samples) or ERCC
576 RNA Spike-In Mix (for all other samples) that provides a set of external RNA controls was
577 added to the total RNA to enable performance assessment. The Spike-Ins were used for
578 quality control purposes, but not used for the final analysis of DGE, DTU or AS.

579 Using the Illumina TruSeq Stranded Total RNA kit library preparation was accomplished. This
580 includes removing ribosomal RNA via biotinylated target-specific oligos combined with Ribo-
581 Zero gold rRNA removal beads from 1 µg total RNA input. Cytoplasmic and mitochondrial
582 rRNA gets depleted by the Ribo-Zero Human/Mouse/Rat kit. After a purification step, the RNA
583 gets cleaved and fragmented. These fragments are then reverse transcribed into first strand
584 cDNA using reverse transcriptase and random primers. In the next step, using DNA
585 Polymerase I and RNase H second strand cDNA synthesis is performed. The resulting cDNA
586 fragments then have the extension of a single'A' base and adapter ligation. To create the final
587 cDNA library the products are purified and enriched with PCR. Next library validation and
588 quantification (Agilent tape station) are performed, followed by pooling of equimolar amounts
589 of library. The pool itself was then quantified using the Peqlab KAPA Library Quantification Kit
590 and the Applied Biosystems 7900HT Sequence Detection System and sequenced on an
591 Illumina HiSeq4000 sequencing instrument with an PE75 protocol (UPF3B KO samples) or
592 Illumina NovaSeq6000 sequencing instrument with an PE100 protocol (all other samples).

593 Reads were aligned against the human genome (version 38, GENCODE release 33 transcript
594 annotations (Frankish *et al.*, 2019) supplemented with SIRVomeERCCome annotations from

595 Lexogen; obtained from https://www.lexogen.com/sirvs/download/) using the STAR read
596 aligner (version 2.7.3a) (Dobin *et al.*, 2013). Transcript abundance estimates were computed
597 with Salmon (version 1.3.0) (Patro *et al.*, 2017) with a decoy-aware transcriptome. After the
598 import of transcript abundances, differential gene expression analysis was performed with the
599 DESeq2(Love *et al.*, 2014) R package (version 1.28.1) with the significance thresholds
600 |log2FoldChange|> 1 and adjusted p-value (padj) < 0.05. Differential splicing was detected with
601 LeafCutter (version 0.2.9) (Li *et al.*, 2018) with the significance thresholds |deltapsi| > 0.1 and
602 adjusted p-value (p.adjust) < 0.05. Differential transcript usage was computed with
603 IsoformSwitchAnalyzeR (version 1.10.0) and the DEXSeq method (Anders *et al.*, 2012; Ritchie
604 *et al.*, 2015; Robinson & Oshlack, 2010; Soneson *et al.*, 2015; Vitting-Seerup & Sandelin, 2017,
605 2019). Significance thresholds were |dIF| > 0.1 and adjusted p-value (isoform_switch_q_value)
606 < 0.05.

607 PTC status of transcript isoforms with annotated open reading frame was determined by
608 IsoformSwitchAnalyzeR using the 50 nucleotide (nt) rule of NMD (Huber *et al.*, 2015; Vitting-
609 Seerup *et al.*, 2014; Vitting-Seerup & Sandelin, 2017; Weischenfeldt *et al.*, 2012). Isoforms
610 with no annotated open reading frame in GENCODE were designated “NA” in the PTC
611 analysis.

612 All scripts and parameters for the RNA-Seq analysis are available at GitHub
613 [https://github.com/boehmv/UPF3]. Overlaps of data sets were represented via nVenn(Perez-
614 Silva *et al.*, 2018) or the ComplexHeatmap package (version 2.6.2)(Gu *et al.*, 2016). Integrative
615 Genomics Viewer (IGV) (version 2.8.12)(Robinson *et al.*, 2011) snapshots were generated
616 from mapped reads (BAM files) converted to binary tiled data (tdf), using Alfred(Rausch *et al.*,
617 2019) with resolution set to 1 and IGVtools.

618 **SILAC and mass spectrometry**

619 HEK293 WT cells and the UPF3 dKO clone 2 expressing either FLAG-tagged GST or UPF2
620 were labeled by culturing them for at least 5 passages in DMEM for SILAC medium (Thermo
621 Fisher Scientific) supplemented with 9% FBS (Silantes), 1% Penicillin-Streptomycin and the

622 labeled amino acids Lysin and Arginine at final concentrations of 0.798 mmol/L and 0.393
623 mmol/L, respectively. The three conditions were “light” (unlabeled Lys/ Arg), “medium” (Lys4/
624 Arg6) and “heavy” (Lys8/ Arg10). Unlabeled proline was added in all conditions to prevent
625 enzymatic Arginine-to-Proline conversion.

626 **Experimental setup for SILAC with FLAG-tagged UPF2**

627 Expression of FLAG-GST and FLAG-UPF2 was induced for 72 h with 1x cumate. The cells
628 lysed in 250 – 400 µl Buffer E with 1 µg/ml RNase and sonicated using the Bandelin Sonopuls
629 mini20 with 15x 1s pulses at 50% amplitude with a 2.5 mm tip. Protein concentrations were
630 measured using the Bradford assay and protein samples containing 1.6-1.7 mg/ml total protein
631 were diluted. 600 µl of these samples were incubated with 30 µl Anti-FLAG M2 magnetic beads
632 (Sigma) for 2 h on an overhead shaker at 4 °C. The beads were then washed three times for
633 5 min with mild EJC-Buffer before eluting twice with 22 µl of a 200 µg/ml dilution of FLAG-
634 peptides (Sigma) in 1x TBS for 10 min at RT and 200 rpm each elution step. Another elution
635 with 1x SDS loading buffer was performed to analyze pull down efficiency via Western blot.
636 The FLAG-peptide eluates were then mixed as followed: 7 µl of both light conditions, 14 µl
637 medium and 14 µl heavy. 1 volume of SP3 (10% SDS in PBS) was added and the samples
638 were reduced with 5 mM DTT and alkylated with 40 mM CAA.

639 Tryptic protein digestion was achieved by following a modified version of the single pot solid
640 phase-enhanced sample preparation (SP3) (Hughes *et al.*, 2014). In brief, paramagnetic Sera-
641 Mag speed beads (Thermo Fisher Scientific) were added to the reduced and alkylated protein
642 samples and then mixed 1:1 with 100% acetonitrile (ACN). Protein-beads-complexes form
643 during the 8 min incubation step, followed by capture using an in-house build magnetic rack.
644 After two washing steps with 70% EtOH, the samples were washed once with 100% ACN.
645 Then they were air-dried, resuspended in 5 µl 50 mM Triethylamonium bicarbonate
646 supplemented with trypsin and LysC in an enzyme:substrate ratio of 1:50 and incubated for 16
647 h at 37°C. The next day the beads were again resuspended in 200 µl ACN and after 8 min
648 incubation placed on the magnetic rack. Tryptic peptides were washed with 100% ACN and

649 air-dried before dissolved in 4% DMSO and transfer into 96-well PCR tubes. The last step was
650 the acidification with 1 µl of 10% formic acid, then the samples were ready for mass spec
651 analysis.

652 Proteomics analysis was performed by the proteomics core facility at CECAD via data-
653 dependent acquisition using an Easy nLC1200 ultra high-performance liquid chromatography
654 (UHPLC) system connected via nano electrospray ionization to a Q Exactive Plus instrument
655 (all Thermo Scientific) running in DDA Top10 mode. Based on their hydrophobicity the tryptic
656 peptides were separated using a chromatographic gradient of 60 min with a binary system of
657 buffer A (0.1% formic acid) and buffer B (80% ACN, 0.1% formic acid) with a total flow of 250
658 nl/min. For the separation in-house made analytical columns (length: 50 cm, inner diameter:
659 75 µm) containing 2.7 µm C18 Poroshell EC120 beads (Agilent) that were heated to 50 °C in
660 a column oven (Sonation) were used. Over a time period of 41 min Buffer B was linearly
661 increased from 3% to 27% and then more rapidly up to 50% in 8 min. Finally, buffer B was
662 increased to 95% within 1 min followed by 10 min at 95% to wash the analytical column. Full
663 MS spectra (300-1,750 m/z) were accomplished with a resolution of 70,000, a maximum
664 injection time of 20 ms and an AGC target of 3e6. In each full MS spectrum, the top 10 most
665 abundant ions were selected for HCD fragmentation (NCE:27) with a quadrupole isolation
666 width of 1.8 m/z and 10 s dynamic exclusion. The MS/MS spectra were then measured with a
667 35,000 resolution, an injection time of maximum 110 ms and an AGC target of 5e5.

668 The MS RAW files were then analyzed with MaxQuant suite (version 1.5.3.8) on standard
669 settings with the before mentioned SILAC labels (Cox & Mann, 2008). By matching against the
670 human UniProt database the peptides were then identified using the Andromeda scoring
671 algorithm (Cox *et al.*, 2011). Carbamidomethylation of cysteine was defined as a fixed
672 modification, while methionine oxidation and N-terminal acetylation were variable
673 modifications. The digestion protein was Trypsin/P. A false discovery rate (FDR) < 0.01 was
674 used to identify peptide-spectrum matches and to quantify the proteins. Data processing and
675 statistical analysis was performed in the Perseus software (version 1.6.1.1) (Tyanova *et al.*,

676 2016). Using the One-sample t-test the significantly changed proteins were identified (H0 = 0,
677 fudge factor S0 = 0.2). Visualization was performed with RStudio (version 1.2.5033).

678 **Label-free quantitative mass spectrometry**

679 Twenty-four hours before expression of the FLAG-tagged constructs, the HEK293 WT cells
680 were treated with Luciferase siRNA and the UPF3B KO clone 90 and UPF3 dKO clone 1 cells
681 were treated with siRNAs targeting residual UPF3B. The expression of either FLAG-GST or
682 FLAG-UPF2 in WT cells and FLAG-UPF2 in the clones 90 and 1 was induced for 48 h with 1x.
683 Lysis and sample preparation were performed as described above. MS analysis was
684 performed as described above with a slightly adjusted gradient as followed: 3 – 30% B in 41
685 min, 30 – 50% B in 8 min, 50-95% B in 1 min, followed by 10 min washing at 95%. LFQ values
686 were calculated using the MaxLFQ algorithm (Cox *et al.*, 2014) in MaxQuant. Significantly
687 changed proteins were identified by two-sample *t*-testing (fudge factor S0 = 0.2).

688 **Northern Blotting**

689 The cells were harvested in RNAsolv reagent and total RNA extraction was performed as
690 described above. 3.0 µg total RNA were resolved on a 1% agarose/0.4 M formaldehyde gel
691 using the tricine/triethanolamine buffer system (Mansour & Pestov, 2013). Next a transfer on
692 a nylon membrane (Roth) in 10x SSC followed. The blot was incubated overnight at 65°C in
693 Church buffer containing [α-32P]-GTP body-labeled RNA-probes for mRNA reporter detection
694 (Voigt *et al.*, 2019). Ethidium bromide stained 28S and 18S rRNA served as loading controls.
695 RNA signal detected with the Typhoon FLA 7000 (GE Healthcare) was quantified in a semi-
696 automated manner using the ImageQuant TL 1D software with a rolling-ball background
697 correction. EtBr-stained rRNA bands were quantified with the Image Lab 6.0.1 software (Bio-
698 Rad). Signal intensities were normalized to the internal control (rRNA) before calculation of
699 mean values. The control condition was set to unity (TPI WT for reporter assays), quantification
700 results are shown as data points and mean.

701 **Protein conservation**

702 UPF3A (UniProt ID: Q9H1J1-1) and UPF3B (UniProt ID: Q9BZI7-2) protein sequences were
703 aligned using Clustal Omega (https://www.ebi.ac.uk/Tools/msa/clustalo/) (Goujon *et al.*, 2010;
704 Sievers *et al.*, 2011), viewed using Jalview (Waterhouse *et al.*, 2009), the conservation score
705 extracted and used for visualization.

706 **Data Presentation**

707 Quantifications and calculations for other experiments were performed - if not indicated
708 otherwise - with Microsoft Excel (version 1808) or R (version 4.0.4) and all plots were
709 generated using IGV (version 2.8.12), GraphPad Prism 5, ggplot2 (version 3.3.3) or
710 ComplexHeatmap (version 2.6.2) (Gu *et al.*, 2016).

711 **Data Availability**

712 The datasets and computer code produced in this study are available in the following
713 databases:

714 - RNA-Seq data for UPF3B KO samples: ArrayExpress E-MTAB-10711
715 (https://www.ebi.ac.uk/arrayexpress/experiments/E-MTAB-10711)
716 - RNA-Seq data for UPF3 dKO samples: ArrayExpress E-MTAB-10716
717 (https://www.ebi.ac.uk/arrayexpress/experiments/E-MTAB-10716)
718 - RNA-Seq data for UPF3A KO/OE samples: ArrayExpress E-MTAB-10718
719 (https://www.ebi.ac.uk/arrayexpress/experiments/E-MTAB-10718)
720 - Mass spectrometry proteomics data: PRIDE PXD027120
721 (https://www.ebi.ac.uk/pride/archive/projects/PXD027120)
722 - Codes used in this study: GitHub (https://github.com/boehmv/UPF3)

723 All relevant data supporting the key findings of this study are available within the article and its
724 Expanded View files or from the corresponding author upon reasonable request.

Acknowledgements

We thank members of the Gehring lab for discussions and reading of the manuscript. We also thank Marek Franitza and Christian Becker (Cologne Center for Genomics, CCG) for preparing the sequencing libraries and operating the sequencer. This work was supported by grants from the Deutsche Forschungsgemeinschaft to C.D. (DI 1501/8-1, DI1501/8-2) and N.H.G (GE 2014/6-2 and GE 2014/10-1) and by the Center for Molecular Medicine Cologne (CMMC, Project C 07; to N.H.G.). V.B. was funded under the Institutional Strategy of the University of Cologne within the German Excellence Initiative. N.H.G. acknowledges funding by a Heisenberg professorship (GE 2014/7-1 and GE 2014/13-1) from the Deutsche Forschungsgemeinschaft. C.D was kindly supported by the Klaus Tschira Stiftung gGmbH (00.219.2013). This work was supported by the DFG Research Infrastructure as part of the Next Generation Sequencing Competence Network (project 423957469). NGS analyses were carried out at the production site WGGC Cologne.

Author contributions

Conceptualization: Niels H. Gehring, Volker Boehm and Damaris Wallmeroth;

Methodology: Volker Boehm, Damaris Wallmeroth, Niels H. Gehring;

Software: Volker Boehm;

Investigation: Damaris Wallmeroth, Volker Boehm, and Jan-Wilm Lackmann;

Resources and Data Curation: Volker Boehm, Janine Altmüller and Jan-Wilm Lackmann;

Writing – Original Draft, Review & Editing: Damaris Wallmeroth, Volker Boehm, Niels H. Gehring;

Visualization: Volker Boehm and Damaris Wallmeroth;

Supervision: Niels H. Gehring and Volker Boehm;

Funding Acquisition: Niels H. Gehring and Christoph Dieterich;

750 ## Conflict of interest

751 None.

752 # References

753 Amrani N, Ganesan R, Kervestin S, Mangus DA, Ghosh S, Jacobson A (2004) A faux 3'-UTR
754 promotes aberrant termination and triggers nonsense-mediated mRNA decay. *Nature* 432:
755 112-118

756 Anders S, Reyes A, Huber W (2012) Detecting differential usage of exons from RNA-seq data.
757 *Genome Res* 22: 2008-2017

758 Boehm V, Gerbracht JV, Marx MC, Gehring NH (2016) Interrogating the degradation pathways
759 of unstable mRNAs with XRN1-resistant sequences. *Nat Commun* 7: 13691

760 Boehm V, Kueckelmann S, Gerbracht JV, Kallabis S, Britto-Borges T, Altmuller J, Kruger M,
761 Dieterich C, Gehring NH (2021) SMG5-SMG7 authorize nonsense-mediated mRNA decay by
762 enabling SMG6 endonucleolytic activity. *Nat Commun* 12: 3965

763 Bono F, Ebert J, Unterholzner L, Guttler T, Izaurralde E, Conti E (2004) Molecular insights into
764 the interaction of PYM with the Mago-Y14 core of the exon junction complex. *EMBO Rep* 5:
765 304-310

766 Buchwald G, Ebert J, Basquin C, Sauliere J, Jayachandran U, Bono F, Le Hir H, Conti E (2010)
767 Insights into the recruitment of the NMD machinery from the crystal structure of a core EJC-
768 UPF3b complex. *Proc Natl Acad Sci U S A* 107: 10050-10055

769 Chamieh H, Ballut L, Bonneau F, Le Hir H (2008) NMD factors UPF2 and UPF3 bridge UPF1
770 to the exon junction complex and stimulate its RNA helicase activity. *Nat Struct Mol Biol* 15:
771 85-93

772 Chan WK, Bhalla AD, Le Hir H, Nguyen LS, Huang L, Gecz J, Wilkinson MF (2009) A UPF3-
773 mediated regulatory switch that maintains RNA surveillance. *Nat Struct Mol Biol* 16: 747-753

774 Chen CY, Shyu AB (2003) Rapid deadenylation triggered by a nonsense codon precedes
775 decay of the RNA body in a mammalian cytoplasmic nonsense-mediated decay pathway. *Mol*
776 *Cell Biol* 23: 4805-4813

777 Cox J, Hein MY, Luber CA, Paron I, Nagaraj N, Mann M (2014) Accurate proteome-wide label-
778 free quantification by delayed normalization and maximal peptide ratio extraction, termed
779 MaxLFQ. *Mol Cell Proteomics* 13: 2513-2526

780 Cox J, Mann M (2008) MaxQuant enables high peptide identification rates, individualized
781 p.p.b.-range mass accuracies and proteome-wide protein quantification. *Nat Biotechnol* 26:
782 1367-1372

783 Cox J, Neuhauser N, Michalski A, Scheltema RA, Olsen JV, Mann M (2011) Andromeda: a
784 peptide search engine integrated into the MaxQuant environment. *J Proteome Res* 10: 1794-
785 1805

786 Dobin A, Davis CA, Schlesinger F, Drenkow J, Zaleski C, Jha S, Batut P, Chaisson M,
787 Gingeras TR (2013) STAR: ultrafast universal RNA-seq aligner. *Bioinformatics* 29: 15-21

788 Dostie J, Dreyfuss G (2002) Translation is required to remove Y14 from mRNAs in the
789 cytoplasm. *Curr Biol* 12: 1060-1067

790 Eberle AB, Lykke-Andersen S, Muhlemann O, Jensen TH (2009) SMG6 promotes
791 endonucleolytic cleavage of nonsense mRNA in human cells. *Nat Struct Mol Biol* 16: 49-55

792 Frankish A, Diekhans M, Ferreira AM, Johnson R, Jungreis I, Loveland J, Mudge JM, Sisu C,
793 Wright J, Armstrong J *et al* (2019) GENCODE reference annotation for the human and mouse
794 genomes. *Nucleic Acids Res* 47: D766-D773

795 Frischmeyer PA, Dietz HC (1999) Nonsense-mediated mRNA decay in health and disease.
796 *Hum Mol Genet* 8: 1893-1900

797 Gehring NH, Lamprinaki S, Kulozik AE, Hentze MW (2009) Disassembly of exon junction
798 complexes by PYM. *Cell* 137: 536-548

799 Gehring NH, Neu-Yilik G, Schell T, Hentze MW, Kulozik AE (2003) Y14 and hUpf3b form an
800 NMD-activating complex. *Mol Cell* 11: 939-949

801 Gerbracht JV, Boehm V, Britto-Borges T, Kallabis S, Wiederstein JL, Ciriello S, Aschemeier
802 DU, Kruger M, Frese CK, Altmuller J *et al* (2020) CASC3 promotes transcriptome-wide
803 activation of nonsense-mediated decay by the exon junction complex. *Nucleic Acids Res* 48:
804 8626-8644

805 Goujon M, McWilliam H, Li W, Valentin F, Squizzato S, Paern J, Lopez R (2010) A new
806 bioinformatics analysis tools framework at EMBL-EBI. *Nucleic Acids Res* 38: W695-699

807 Gu Z, Eils R, Schlesner M (2016) Complex heatmaps reveal patterns and correlations in
808 multidimensional genomic data. *Bioinformatics* 32: 2847-2849

809 He F, Li X, Spatrick P, Casillo R, Dong S, Jacobson A (2003) Genome-wide analysis of mRNAs
810 regulated by the nonsense-mediated and 5' to 3' mRNA decay pathways in yeast. *Mol Cell* 12:
811 1439-1452

812 Hogg JR, Goff SP (2010) Upf1 senses 3'UTR length to potentiate mRNA decay. *Cell* 143: 379-
813 389

814 Huber W, Carey VJ, Gentleman R, Anders S, Carlson M, Carvalho BS, Bravo HC, Davis S,
815 Gatto L, Girke T *et al* (2015) Orchestrating high-throughput genomic analysis with
816 Bioconductor. *Nat Methods* 12: 115-121

817 Hughes CS, Foehr S, Garfield DA, Furlong EE, Steinmetz LM, Krijgsveld J (2014)
818 Ultrasensitive proteome analysis using paramagnetic bead technology. *Mol Syst Biol* 10: 757

819 Huntzinger E, Kashima I, Fauser M, Sauliere J, Izaurralde E (2008) SMG6 is the catalytic
820 endonuclease that cleaves mRNAs containing nonsense codons in metazoan. *RNA* 14: 2609-
821 2617

822 Hurt JA, Robertson AD, Burge CB (2013) Global analyses of UPF1 binding and function reveal
823 expanded scope of nonsense-mediated mRNA decay. *Genome Res* 23: 1636-1650

824 Hwang J, Maquat LE (2011) Nonsense-mediated mRNA decay (NMD) in animal
825 embryogenesis: to die or not to die, that is the question. *Current opinion in genetics &*
826 *development* 21: 422-430

827 Kadlec J, Izaurralde E, Cusack S (2004) The structural basis for the interaction between
828 nonsense-mediated mRNA decay factors UPF2 and UPF3. *Nat Struct Mol Biol* 11: 330-337

829 Kashima I, Yamashita A, Izumi N, Kataoka N, Morishita R, Hoshino S, Ohno M, Dreyfuss G,
830 Ohno S (2006) Binding of a novel SMG-1-Upf1-eRF1-eRF3 complex (SURF) to the exon
831 junction complex triggers Upf1 phosphorylation and nonsense-mediated mRNA decay. *Genes*
832 *Dev* 20: 355-367

833 Kervestin S, Jacobson A (2012) NMD: a multifaceted response to premature translational
834 termination. *Nature reviews Molecular cell biology* 13: 700-712

835 Kim VN, Kataoka N, Dreyfuss G (2001) Role of the nonsense-mediated decay factor hUpf3 in
836 the splicing-dependent exon-exon junction complex. *Science* 293: 1832-1836

837 Kunz JB, Neu-Yilik G, Hentze MW, Kulozik AE, Gehring NH (2006) Functions of hUpf3a and
838 hUpf3b in nonsense-mediated mRNA decay and translation. *RNA* 12: 1015-1022

839 Kurosaki T, Maquat LE (2013) Rules that govern UPF1 binding to mRNA 3' UTRs. *Proc Natl*
840 *Acad Sci U S A* 110: 3357-3362

841 Le Hir H, Gatfield D, Izaurralde E, Moore MJ (2001) The exon-exon junction complex provides
842 a binding platform for factors involved in mRNA export and nonsense-mediated mRNA decay.
843 *EMBO J* 20: 4987-4997

844 Le Hir H, Izaurralde E, Maquat LE, Moore MJ (2000) The spliceosome deposits multiple
845 proteins 20-24 nucleotides upstream of mRNA exon-exon junctions. *EMBO J* 19: 6860-6869

846 Lejeune F, Li X, Maquat LE (2003) Nonsense-mediated mRNA decay in mammalian cells
847 involves decapping, deadenylating, and exonucleolytic activities. *Mol Cell* 12: 675-687

848 Lelivelt MJ, Culbertson MR (1999) Yeast Upf proteins required for RNA surveillance affect
849 global expression of the yeast transcriptome. *Mol Cell Biol* 19: 6710-6719

850 Li T, Shi Y, Wang P, Guachalla LM, Sun B, Joerss T, Chen YS, Groth M, Krueger A, Platzer
851 M *et al* (2015) Smg6/Est1 licenses embryonic stem cell differentiation via nonsense-mediated
852 mRNA decay. *EMBO J* 34: 1630-1647

853 Li YI, Knowles DA, Humphrey J, Barbeira AN, Dickinson SP, Im HK, Pritchard JK (2018)
854 Annotation-free quantification of RNA splicing using LeafCutter. *Nat Genet* 50: 151-158

855 Love MI, Huber W, Anders S (2014) Moderated estimation of fold change and dispersion for
856 RNA-seq data with DESeq2. *Genome biology* 15: 550

857 Lykke-Andersen J, Shu MD, Steitz JA (2000) Human Upf proteins target an mRNA for
858 nonsense-mediated decay when bound downstream of a termination codon. *Cell* 103: 1121-
859 1131

860 Lykke-Andersen S, Chen Y, Ardal BR, Lilje B, Waage J, Sandelin A, Jensen TH (2014) Human
861 nonsense-mediated RNA decay initiates widely by endonucleolysis and targets snoRNA host
862 genes. *Genes Dev* 28: 2498-2517

863 Mansour FH, Pestov DG (2013) Separation of long RNA by agarose-formaldehyde gel
864 electrophoresis. *Anal Biochem* 441: 18-20

865 McIlwain DR, Pan Q, Reilly PT, Elia AJ, McCracken S, Wakeham AC, Itie-Youten A, Blencowe
866 BJ, Mak TW (2010) Smg1 is required for embryogenesis and regulates diverse genes via
867 alternative splicing coupled to nonsense-mediated mRNA decay. *Proc Natl Acad Sci U S A*
868 107: 12186-12191

869 Medghalchi SM, Frischmeyer PA, Mendell JT, Kelly AG, Lawler AM, Dietz HC (2001) Rent1, a
870 trans-effector of nonsense-mediated mRNA decay, is essential for mammalian embryonic
871 viability. *Hum Mol Genet* 10: 99-105

872 Melero R, Buchwald G, Castano R, Raabe M, Gil D, Lazaro M, Urlaub H, Conti E, Llorca O
873 (2012) The cryo-EM structure of the UPF-EJC complex shows UPF1 poised toward the RNA
874 3' end. *Nat Struct Mol Biol* 19: 498-505, S491-492

875 Mendell JT, Sharifi NA, Meyers JL, Martinez-Murillo F, Dietz HC (2004) Nonsense surveillance
876 regulates expression of diverse classes of mammalian transcripts and mutes genomic noise.
877 *Nat Genet* 36: 1073-1078

878 Metzstein MM, Krasnow MA (2006) Functions of the nonsense-mediated mRNA decay
879 pathway in Drosophila development. *PLoS Genet* 2: e180

880 Neu-Yilik G, Raimondeau E, Eliseev B, Yeramala L, Amthor B, Deniaud A, Huard K,
881 Kerschgens K, Hentze MW, Schaffitzel C *et al* (2017) Dual function of UPF3B in early and late
882 translation termination. *EMBO J* 36: 2968-2986

883 Nguyen LS, Jolly L, Shoubridge C, Chan WK, Huang L, Laumonnier F, Raynaud M, Hackett
884 A, Field M, Rodriguez J *et al* (2012) Transcriptome profiling of UPF3B/NMD-deficient
885 lymphoblastoid cells from patients with various forms of intellectual disability. *Mol Psychiatry*
886 17: 1103-1115

887 Nguyen LS, Wilkinson MF, Gecz J (2014) Nonsense-mediated mRNA decay: inter-individual
888 variability and human disease. *Neurosci Biobehav Rev* 46 Pt 2: 175-186

889 Patro R, Duggal G, Love MI, Irizarry RA, Kingsford C (2017) Salmon provides fast and bias-
890 aware quantification of transcript expression. *Nat Methods* 14: 417-419

891 Peixeiro I, Inacio A, Barbosa C, Silva AL, Liebhaber SA, Romao L (2012) Interaction of
892 PABPC1 with the translation initiation complex is critical to the NMD resistance of AUG-
893 proximal nonsense mutations. *Nucleic Acids Res* 40: 1160-1173

894 Perez-Silva JG, Araujo-Voces M, Quesada V (2018) nVenn: generalized, quasi-proportional
895 Venn and Euler diagrams. *Bioinformatics* 34: 2322-2324

896 Rausch T, Hsi-Yang Fritz M, Korbel JO, Benes V (2019) Alfred: interactive multi-sample BAM
897 alignment statistics, feature counting and feature annotation for long- and short-read
898 sequencing. *Bioinformatics* 35: 2489-2491

899 Rehwinkel J, Letunic I, Raes J, Bork P, Izaurralde E (2005) Nonsense-mediated mRNA decay
900 factors act in concert to regulate common mRNA targets. *RNA* 11: 1530-1544

901 Ritchie ME, Phipson B, Wu D, Hu Y, Law CW, Shi W, Smyth GK (2015) limma powers
902 differential expression analyses for RNA-sequencing and microarray studies. *Nucleic Acids*
903 *Res* 43: e47

904 Robinson JT, Thorvaldsdottir H, Winckler W, Guttman M, Lander ES, Getz G, Mesirov JP
905 (2011) Integrative genomics viewer. *Nat Biotechnol* 29: 24-26

906 Robinson MD, Oshlack A (2010) A scaling normalization method for differential expression
907 analysis of RNA-seq data. *Genome biology* 11: R25

908 Serin G, Gersappe A, Black JD, Aronoff R, Maquat LE (2001) Identification and
909 characterization of human orthologues to Saccharomyces cerevisiae Upf2 protein and Upf3
910 protein (Caenorhabditis elegans SMG-4). *Mol Cell Biol* 21: 209-223

911 Shum EY, Jones SH, Shao A, Dumdie J, Krause MD, Chan WK, Lou CH, Espinoza JL, Song
912 HW, Phan MH *et al* (2016) The Antagonistic Gene Paralogs Upf3a and Upf3b Govern
913 Nonsense-Mediated RNA Decay. *Cell* 165: 382-395

914 Sievers F, Wilm A, Dineen D, Gibson TJ, Karplus K, Li W, Lopez R, McWilliam H, Remmert M,
915 Soding J *et al* (2011) Fast, scalable generation of high-quality protein multiple sequence
916 alignments using Clustal Omega. *Mol Syst Biol* 7: 539

917 Soneson C, Love MI, Robinson MD (2015) Differential analyses for RNA-seq: transcript-level
918 estimates improve gene-level inferences. *F1000Res* 4: 1521

919 Sureau A, Gattoni R, Dooghe Y, Stevenin J, Soret J (2001) SC35 autoregulates its expression
920 by promoting splicing events that destabilize its mRNAs. *EMBO J* 20: 1785-1796

921 Tyanova S, Temu T, Sinitcyn P, Carlson A, Hein MY, Geiger T, Mann M, Cox J (2016) The
922 Perseus computational platform for comprehensive analysis of (prote)omics data. *Nat Methods*
923 13: 731-740

924 Vitting-Seerup K, Porse BT, Sandelin A, Waage J (2014) spliceR: an R package for
925 classification of alternative splicing and prediction of coding potential from RNA-seq data. *BMC*
926 *Bioinformatics* 15: 81

927 Vitting-Seerup K, Sandelin A (2017) The Landscape of Isoform Switches in Human Cancers.
928 *Mol Cancer Res* 15: 1206-1220

929 Vitting-Seerup K, Sandelin A (2019) IsoformSwitchAnalyzeR: analysis of changes in genome-
930 wide patterns of alternative splicing and its functional consequences. *Bioinformatics* 35: 4469-
931 4471

932 Voigt F, Gerbracht JV, Boehm V, Horvathova I, Eglinger J, Chao JA, Gehring NH (2019)
933 Detection and quantification of RNA decay intermediates using XRN1-resistant reporter
934 transcripts. *Nat Protoc* 14: 1603-1633

935 Waterhouse AM, Procter JB, Martin DM, Clamp M, Barton GJ (2009) Jalview Version 2--a
936 multiple sequence alignment editor and analysis workbench. *Bioinformatics* 25: 1189-1191

937 Weischenfeldt J, Damgaard I, Bryder D, Theilgaard-Monch K, Thoren LA, Nielsen FC,
938 Jacobsen SE, Nerlov C, Porse BT (2008) NMD is essential for hematopoietic stem and
939 progenitor cells and for eliminating by-products of programmed DNA rearrangements. *Genes*
940 *Dev* 22: 1381-1396

941 Weischenfeldt J, Waage J, Tian G, Zhao J, Damgaard I, Jakobsen JS, Kristiansen K, Krogh
942 A, Wang J, Porse BT (2012) Mammalian tissues defective in nonsense-mediated mRNA decay
943 display highly aberrant splicing patterns. *Genome biology* 13: R35

944 Weng Y, Czaplinski K, Peltz SW (1996) Identification and characterization of mutations in the
945 UPF1 gene that affect nonsense suppression and the formation of the Upf protein complex but
946 not mRNA turnover. *Mol Cell Biol* 16: 5491-5506

947 Wittkopp N, Huntzinger E, Weiler C, Sauliere J, Schmidt S, Sonawane M, Izaurralde E (2009)
948 Nonsense-mediated mRNA decay effectors are essential for zebrafish embryonic development
949 and survival. *Mol Cell Biol* 29: 3517-3528

950 Yamashita A, Ohnishi T, Kashima I, Taya Y, Ohno S (2001) Human SMG-1, a novel
951 phosphatidylinositol 3-kinase-related protein kinase, associates with components of the mRNA

952 surveillance complex and is involved in the regulation of nonsense-mediated mRNA decay.
953 *Genes Dev* 15: 2215-2228

954 Yi Z, Arvola RM, Myers S, Dilsavor CN, Abu Alhasan R, Carter BN, Patton RD, Bundschuh R,
955 Singh G (2021) Mammalian UPF3A and UPF3B activate NMD independently of their EJC
956 binding. *bioRxiv*: 2021.2007.2002.450872

957 Zund D, Gruber AR, Zavolan M, Muhlemann O (2013) Translation-dependent displacement of
958 UPF1 from coding sequences causes its enrichment in 3' UTRs. *Nat Struct Mol Biol* 20: 936-
959 943

960